NAVAL POSTGRADUATE SCHOOL

MONTEREY, CALIFORNIA

THESIS

ANALYSIS OF LATERAL BOUNDARY EFFECTS ON INNER DOMAIN OF COAMPS

by

Brad G. Harris

September 2004

Thesis Co-Advisors: Douglas K. Miller
                        Beny Neta

Approved for public release; distribution is unlimited.

THIS PAGE INTENTIONALLY LEFT BLANK

1. AGENCY USE ONLY (*Leave blank*)	2. REPORT DATE September 2004	3. REPORT TYPE AND DATES COVERED Master's Thesis	

4. TITLE AND SUBTITLE: Analysis of Lateral Boundary Effects on Inner Domain of COAMPS	**5. FUNDING NUMBERS**
6. AUTHOR(S) Brad G. Harris	
7. PERFORMING ORGANIZATION NAME(S) AND ADDRESS(ES) Naval Postgraduate School Monterey, CA 93943-5000	**8. PERFORMING ORGANIZATION REPORT NUMBER**
9. SPONSORING /MONITORING AGENCY NAME(S) AND ADDRESS(ES) N/A	**10. SPONSORING/MONITORING AGENCY REPORT NUMBER**

11. SUPPLEMENTARY NOTES The views expressed in this thesis are those of the author and do not reflect the official policy or position of the Department of Defense or the U.S. Government.

12a. DISTRIBUTION / AVAILABILITY STATEMENT Approved for public release; distribution is unlimited.	**12b. DISTRIBUTION CODE**

13. ABSTRACT (maximum 200 words)

One of the major problems with a Limited Area Model is the introduction of error from the lateral boundaries. The boundary condition provides a source of forcing to the interior of the model. This forcing typically originates from a global model such as NOGAPS. The transition at the boundary from one model to another invariably produces errors. Traditionally, the way to minimize boundary error is to move the boundary as far away from the area of interest as possible. In this way, the errors do not have time to infest the LAM with "bad" information. Moving the boundary far away from the area of interest increases the computational forecast load and decreases its timeliness. This study looks at how close the lateral boundary can be to minimize computational time and still maintain a forecast that is useful. It was found that when the entire inner COAMPS nest was analyzed, the differences between the control forecast and the test forecast where within the natural variability of the control grid. It was also found that there where localized areas within the model domain that differed between the control domain and the test domain by up to 20 mb for the sea level pressure after a six day forecast.

14. SUBJECT TERMS COAMPS, Limited Area Models, Lateral Boundary Conditions			15. NUMBER OF PAGES 104
			16. PRICE CODE

17. SECURITY CLASSIFICATION OF REPORT Unclassified	18. SECURITY CLASSIFICATION OF THIS PAGE Unclassified	19. SECURITY CLASSIFICATION OF ABSTRACT Unclassified	20. LIMITATION OF ABSTRACT UL

THIS PAGE INTENTIONALLY LEFT BLANK

**ANALYSIS OF LATERAL BOUNDARY EFFECTS
ON INNER DOMAIN OF COAMPS**

Brad G. Harris
Lieutenant, United States Navy
B.S., Oregon State University, 1995

Submitted in partial fulfillment of the
requirements for the degree of

**MASTER OF SCIENCE IN METEOROLOGY AND PHYSICAL
OCEANOGRAPHY**

and

MASTER OF SCIENCE IN APPLIED MATHEMATICS

from the

**NAVAL POSTGRADUATE SCHOOL
September 2004**

Author: Brad G. Harris

Approved by: Douglas K. Miller
                     Thesis Co-Advisor

                     Beny Neta
                     Thesis Co-Advisor

                     Philip A. Durkee
                     Chairman, Department of Meteorology

                     Clyde Scandrett
                     Chairman, Department of Applied Mathematics

THIS PAGE INTENTIONALLY LEFT BLANK

ABSTRACT

One of the major problems with a Limited Area Model is the introduction of error from the lateral boundaries. The boundary condition provides a source of forcing to the interior of the model. This forcing typically originates from a global model such as NOGAPS. The transition at the boundary from one model to another invariably produces errors. Traditionally, the way to minimize boundary error is to move the boundary as far away from the area of interest as possible. In this way, the errors do not have time to infest the LAM with "bad" information. Moving the boundary far away from the area of interest increases the computational forecast load and decreases its timeliness. This study looks at how close the lateral boundary can be to minimize computational time and still maintain a forecast that is useful. It was found that when the entire inner COAMPS nest was analyzed, the differences between the control forecast and the test forecast where within the natural variability of the control grid. It was also found that there where localized areas within the model domain that differed between the control domain and the test domain by up to 20 mb for the sea level pressure after a six day forecast.

THIS PAGE INTENTIONALLY LEFT BLANK

TABLE OF CONTENTS

LIST OF FIGURES

THIS PAGE INTENTIONALLY LEFT BLANK

LIST OF TABLES

THIS PAGE INTENTIONALLY LEFT BLANK

ACKNOWLEDGMENTS

Special thanks go out to my advisors. Professor Douglas K. Miller provided me with considerable help with the research and composition of this thesis. Professor Beny Neta provided the valuable groundwork for this project, and worked closely with me to ensure fulfillment of the requirements for an M.S. degree in Applied Mathematics.

Special thanks to Roger Stocker who was my point of contact with Fleet Numerical Meteorology and Oceanography Center. Roger let me incorporate my research with work he was doing on COAMPS operation boundary conditions, then helped me move that data from FNMOC to NPS where I could more easily work.

Additional thanks to Bob Creasey, who bailed me out when I got stuck with UNIX. Thanks Bob.

Last but not least, very special thanks go out to my family, Jen, Quentin, Rachael and Sydney, for giving me the love, support and time necessary to complete this phase of my education.

THIS PAGE INTENTIONALLY LEFT BLANK

I.   INTRODUCTION

One of the difficulties with Limited Area Models (LAM) is the treatment of the Lateral Boundary Conditions (LBC). In a global model, the domain size encompasses a spherical globe and there are no boundaries. The equations for the mathematical model are closed in the sense that there are no lateral boundary conditions. With such a large geographical area to cover, high resolution models cannot adequately simulate mesoscale weather features. The model run would be computationally intensive and operationally inhibitive. LAMs are required to capture mesoscale phenomena influenced by the local terrain and local area conditions. One such LAM is the Navy's Coupled Ocean/Atmosphere Mesoscale Prediction System (COAMPS). COAMPS (*Hodur, 1997*), obtains its LBC from the Navy Operational Global Atmospheric Prediction System (NOGAPS), (*Hogan and Rosmond, 1991*).

According to *Warner et al. (1997)* the LBC can influence the resultant solution of a LAM based on the treatment of the following factors. 1) Interpolation; the LBCs are based on the forecast of a coarser resolution model. The horizontal, vertical, and temporal resolution of the boundary information is generally poorer than the LAM. This necessitates the interpolation of boundary information onto the finer grid model domain. For NOGAPS and the COAMPS 81km nest, the grid sizes are nearly the same. Even so, the geographical location of the grid point may not be coincident, so interpolation would still be required. 2) Incorrect data; the model forecast provided from the coarser grid domain may simply be incorrect. Incorrect data could occur due to the model not handling the true weather correctly, or because there is a meteorological phenomenon on the boundary of the LAM that the coarse grid model is not designed to handle. 3) One-way interactions; longer wavelengths generated or modified within the LAM cannot feedback to the coarse grid model. In other words, the solution to the LAM may modify the forecast outcome of the global model which, in turn, provides the boundary condition of the LAM. With a one-way interaction, this feedback is not considered. 4) Transient modes; specific LBC schemes can produce transient non-meteorological gravity-inertia

modes on the LAM domain. These transient waves may confuse the interpretation of the LAM forecast. 5) Parameterizations; the coarse and fine grid models may differ in their handling of physical-process parameterizations. The resulting differences in the solutions at the boundary result in spurious gradients between the two grids.

Any errors generated on the boundary will propagate into the interior of the LAM along with the mean flow of the model. Although the magnitude of the influence of the errors will depend on factors such as the strength of the cross-boundary flow, strength of the forcing at the lateral boundaries and the length of the integration, errors in the LBC will influence the resulting forecast. To mitigate lateral boundary errors, conventional wisdom has been to move the lateral boundary as far away from the forecast area of interest (*Warner et al*, 1997). At this point the question arises of how close can the outer boundaries be placed to minimize computational time, yet far enough away to minimize the adverse effects of the boundary.

A.   BACKGROUND

1.   The Fundamental Equations

The three fundamental laws that govern atmospheric motion are conservation of mass, conservation of momentum and conservation of energy. With the proper treatment of these fundamental laws, the behavior of a parcel of air can be described and predicted to a certain degree. By applying these laws, a relatively straightforward set of fundamental equations can be derived and used to describe the synoptic, meso- and microscale fluid motions in the atmosphere.

a.   The Equations of Motion

In order to apply the conservation laws to the atmosphere, it is convenient to start with an analysis of the fundamental forces influencing the motions of air parcels. The first of these forces is the gravitational force. Gravity is a *body force;* the force depends on its mass and acts at the center of the body. Although gravitational force exists between all bodies, the dominant interaction for a parcel of air is between itself and the earth. This interaction can be express as

$$\frac{\mathbf{F_g}}{m} \equiv \mathbf{g*} = -\frac{GM}{r^2}\left(\frac{\mathbf{r}}{r}\right) \tag{0.1}$$

where $\mathbf{g*}$ can be considered a constant.

The second force to consider is the pressure gradient force (PGF). The PGF is an example of a *surface force* because it is independent of the mass and only depends on the surface characteristics. The PGF arises due to the molecular kinetic interaction between the particles within a volume. To analyze the PGF
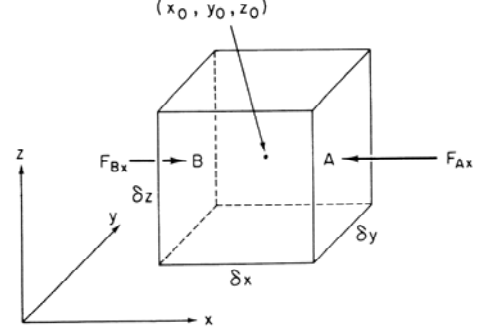
Figure 1   Pressure force acting on left and right face of a unit cube. (*From Holton 1972*)

acting on a parcel of air we consider an infinitesimal volume element $\delta V = \delta x \delta y \delta z$ centered at the point x_o, y_o, and z_o seen in Figure 1. If the pressure in the center of the volume is p_o, then the pressure an infinitesimal distance away from the origin can be expressed as a Taylor series expansion.

$$p = p_o + \frac{\delta p}{\delta x}\frac{\delta x}{2} + \frac{\delta p}{\delta y}\frac{\delta y}{2} + \frac{\delta p}{\delta z}\frac{\delta z}{2} + \text{higher-order terms}$$

Here the non-linear and the higher order terms have been ignored. The pressure force acting on a volume of air on side B in the x direction is:

$$F_{Bx} = -\left(p_o + \frac{\delta p}{\delta x}\frac{\delta x}{2}\right)\delta y \delta z$$

and on side A is:

$$F_{Ax} = +\left(p_o - \frac{\delta p}{\delta x}\frac{\delta x}{2}\right)\delta y \delta z$$

The net pressure force acting on a volume in the x direction is

$$F_x = F_{Ax} + F_{Bx} = -\frac{\delta p}{\delta x}\delta x \delta y \delta z$$

When dividing out the mass and summing the pressure force in all three orientations the combined PGF (per unit mass) becomes

$$\frac{\mathbf{F_{PGF}}}{m} = -\frac{1}{\rho}\nabla p \tag{0.2}$$

where ρ is the mass per unit volume.

The final fundamental force acting on a volume of air is the frictional force. Like the PGF, frictional affects are *surface forces* and do not depend on the mass of the volume. The internal frictional force (viscosity) arises due to a fluid's tendency to resist flow. The simple example is a fluid between two plates, one stationary, the other moving at a
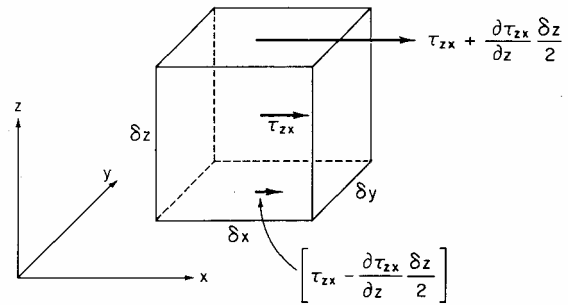
Figure 2 Showing Shearing Stress Acting Tangential to the Surface of a Unit Volume. (*From Holton 1972*)

constant velocity. The fluid adjacent to the stationary plate is at rest relative to the motionless plate. The fluid adjacent to the moving plate is moving at constant velocity with the moving plate. The fluid between the plates must change from a constant velocity next to the moving plate to no motion next to the stationary plate. On the molecular scale, there is a transfer of momentum of the fluid molecules between the plates. By Newton's second law there must be a force associated with this shearing stress to maintain the upper plate in constant motion. The shearing stress is the frictional force and is proportional to the surface area that the sheering stress is acting on. Mathematically, the sheering stress is defined as

$$\tau_{zx} = \mu\frac{\partial u}{\partial z}$$

4

where τ_{zx} is the shearing stress in the x direction owing to the shear normal to the z coordinate, u is the velocity in the x-direction and μ is a constant called the *dynamic viscosity coefficient.*

In the above example there is no net force acting on the system of plates and fluid since the force acting to maintain the top plate in motion is equal and opposite to the force required to maintain the bottom plate stationary. In the more general case of non-steady flow in compressible fluid such as air, a Taylor series expansion can be used again to determine an approximation to the change of the frictional force across a differential volume of air. The stress acting at a point on the top face of the volume in Figure 2 is $\tau_{zx} + \dfrac{\partial \tau_{zx}}{\partial z}\dfrac{\delta z}{2}$ and the stress acting at a point on the bottom face is $-\left[\tau_{zx} - \dfrac{\partial \tau_{zx}}{\partial z}\dfrac{\delta z}{2}\right]$. Therefore the total stress acting on the entire top and bottom face of the volume in Figure 2 is

$$\left(\tau_{zx} + \frac{\partial \tau_{zx}}{\partial z}\frac{\delta z}{2}\right)\delta y \delta x - \left(\tau_{zx} - \frac{\partial \tau_{zx}}{\partial z}\frac{\delta z}{2}\right)\delta y \delta x = \frac{\partial \tau_{zx}}{\partial z}\delta z \delta y \delta x$$

This equation can be divided by the mass of the volume $\rho \delta x \delta y \delta z$ to obtain the viscous force per unit mass owing to vertical shear of the component motion in the x direction is

$$\frac{1}{\rho}\frac{\partial \tau_{zx}}{\partial z} = \frac{1}{\rho}\frac{\partial}{\partial z}\left(\mu \frac{\partial u}{\partial z}\right)$$

Here the dynamic viscosity coefficient is nearly constant and can be combined with the density to become the *kinematic viscosity coefficient, υ.* The above equation simplifies to $\upsilon \dfrac{\partial^2 u}{\partial z^2}$. The resulting frictional force components per unit mass in the three Cartesian coordinate directions are

$$F_{rx} = \upsilon \left[\frac{\partial^2 u}{\partial x^2} + \frac{\partial^2 u}{\partial y^2} + \frac{\partial^2 u}{\partial z^2} \right]$$

$$F_{ry} = \upsilon \left[\frac{\partial^2 v}{\partial x^2} + \frac{\partial^2 v}{\partial y^2} + \frac{\partial^2 v}{\partial z^2} \right] \qquad (0.3)$$

$$F_{rz} = \upsilon \left[\frac{\partial^2 w}{\partial x^2} + \frac{\partial^2 w}{\partial y^2} + \frac{\partial^2 w}{\partial z^2} \right]$$

where *u, v* and *w* are the components of velocity in the *x, y* and *z* directions.

b.   The Momentum Equations

On the synoptic scale of motion, the reference frame for atmospheric motion is the rotating spherical surface of the earth. The fluid motion as observed from the rotating reference frame of the earth's surface appears different than what would be observed from an inertial reference frame such as the earth's center. The change of some quantity *q* with respect to the center of the earth represents the absolute change in the quantity and is expressed as $\frac{Dq}{Dt}$. Locally, fixed on the surface of the earth, that change is expressed as some local differentiation, $\frac{\partial q}{\partial t}$ plus the advection of the quantity on the relative reference system, $\mathbf{v} \cdot \nabla q$. In equation form this becomes:

$$\underbrace{\frac{Dq}{Dt}}_{\text{Absolute change in q}} = \underbrace{\frac{\partial q}{\partial t}}_{\text{Local change in q}} + \underbrace{\mathbf{v} \cdot \nabla q}_{\text{Advection of q}} \qquad (0.4)$$

In an inertial reference frame, Newton's second law of motion states that the sum of the forces acting on a body is equal to the absolute change of the momentum of the body. In this treatment the mass of the body or parcel of air will remain constant so that any net force acting on the air parcel will induce a change in its absolute velocity, **v**.

$$\frac{D\mathbf{v}}{Dt} = \sum \text{real forces acting on parcel} \qquad (0.5)$$

In the inertial reference frame of the earth, there is no apparent rotational affect. There is an apparent deviation in the path of a body or parcel when observed from

6

the rotating reference frame relative to the surface of the earth. Mathematically, the reason for this can be shown by determining the time rate of change of a generic vector quantity **A.**

$$
\begin{aligned}
\frac{D\mathbf{A}}{Dt} &= \frac{dA_x}{dt}\mathbf{i} + \frac{dA_y}{dt}\mathbf{j} + \frac{dA_z}{dt}\mathbf{k} \\
&\quad + A_x\frac{d\mathbf{i}}{dt} + A_y\frac{d\mathbf{j}}{dt} + A_z\frac{d\mathbf{k}}{dt} \\
&= \frac{d\mathbf{A}}{dt} + \Omega \times \mathbf{A}
\end{aligned}
\tag{0.6}
$$

where Ω is the rotational vector of the earth.

In order to determine the time rate of change of the absolute velocity, the absolute change in the radial vector must also be known.

$$
\begin{aligned}
\mathbf{v}_a &= \frac{D\mathbf{r}}{Dt} = \mathbf{v} + \Omega \times \mathbf{r} \\
\frac{D\mathbf{v}_a}{Dt} &= \frac{d}{dt}\left(\mathbf{v} + \Omega \times \mathbf{r}\right) \\
&= \frac{d\mathbf{v}}{dt} + \Omega \times \mathbf{v} + \Omega \times \mathbf{v} + \Omega \times \left(\Omega \times \mathbf{r}\right) \\
&= \frac{d\mathbf{v}}{dt} + \underbrace{2\Omega \times \mathbf{v}}_{\text{Coriols}} - \underbrace{\Omega^2\mathbf{R}}_{\text{Centrifugal}}
\end{aligned}
$$

Here **R** is the position vector from the axis of rotation toward the particle on the surface of the earth. It becomes clear that when the reference frame shifts from the absolute of the earth center to the rotating surface, two apparent forces appear; the Coriolis and the Centrifugal. When summing the forces on the right hand side of equation (0.5), the three real forces that need to be considered are the pressure gradient force, the gravitational force and friction discussed above. It is convenient to combine the gravitational force and the apparent centrifugal force by defining the gravitational force **g** such that

$$
\mathbf{g} \equiv \mathbf{g}^* + \Omega^2\mathbf{R}
$$

Equation (0.5) above now becomes

$$\frac{D\mathbf{v}}{Dt} = -2\Omega \times \mathbf{v} - \frac{1}{\rho}\nabla p + \mathbf{g} + \frac{1}{\rho}\frac{\partial \tau}{\partial z} \tag{0.7}$$

In the familiar Cartesian coordinate system, the velocity vector can be represented by the equation $\mathbf{U} = u\hat{\mathbf{i}} + v\hat{\mathbf{j}} + w\hat{\mathbf{k}}$ where the $\hat{\mathbf{i}}$, $\hat{\mathbf{j}}$ and $\hat{\mathbf{k}}$ are orthogonal unit vectors. When moving from the inertial reference frame of the earth's center to a relative reference frame of the surface, the absolute velocity vector can be represented as

$\mathbf{U} = r\cos\varphi\frac{d\lambda}{dt}\hat{\mathbf{i}} + r\frac{d\varphi}{dt}\hat{\mathbf{j}} + \frac{dr}{dt}\hat{\mathbf{k}}$.

Here $\hat{\mathbf{i}}$, $\hat{\mathbf{j}}$ and $\hat{\mathbf{k}}$ are the new unit

Figure 3   Showing Relationship between Earth Centered Spherical Coordinates and Surface based Cartesian Coordinates.
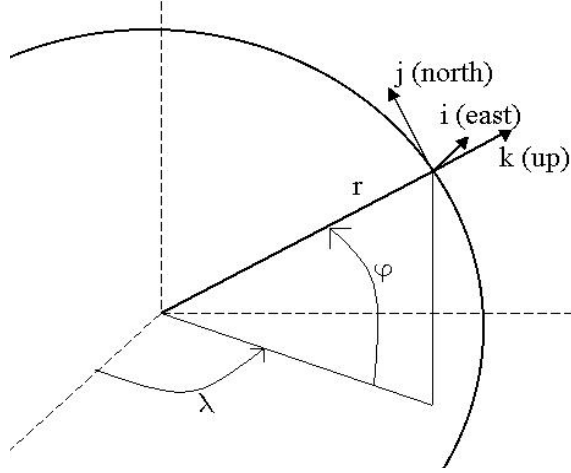
vectors directed toward the east, the north and up respectively. The distance from the center of the earth can be represented by $r = a + z$ where a is the radius of the earth and z is the height above the surface. Since $a \gg z$, r can be replace by a and is considered to be a constant when dealing with atmospheric flow. For notational simplicity, it is convenient to define x as the distance in the easterly direction, y as the distance in the northerly direction and z to point up from the surface.

The velocity vector $\mathbf{v}$ of a body on the relative reference frame of the earth is

$$\mathbf{v} = u\hat{\mathbf{i}} + v\hat{\mathbf{j}} + w\hat{\mathbf{k}}$$

Using equation (0.6), the time rate of change of the velocity vector $\mathbf{v}$ is

8

$$\frac{D\mathbf{v}}{Dt} = \hat{\mathbf{i}}\frac{du}{dt} + \hat{\mathbf{j}}\frac{dv}{dt} + \hat{\mathbf{k}}\frac{dw}{dt} + \Omega \times \mathbf{v}$$

$$= \hat{\mathbf{i}}\left[\frac{du}{dt} - \frac{uv\tan\varphi}{r} + \frac{uw}{r}\right]$$

$$+ \hat{\mathbf{j}}\left[\frac{dv}{dt} + \frac{u^2\tan\varphi}{r} + \frac{vw}{r}\right]$$

$$+ \hat{\mathbf{k}}\left[\frac{dw}{dt} - \frac{u^2}{r} - \frac{v^2}{r}\right]$$

Now equating the right and left hand side of equation (0.7) and combining terms in the three coordinate directions

$$\frac{du}{dt} - \frac{uv\tan\varphi}{r} + \frac{uw}{r} = -\frac{1}{\rho r\cos\varphi}\frac{\partial p}{\partial\lambda} + 2\Omega\left(v\sin\varphi - w\cos\varphi\right) + \frac{1}{\rho}\frac{\partial\tau_\lambda}{\partial r}$$

$$\frac{dv}{dt} + \frac{u^2\tan\varphi}{r} + \frac{vw}{r} = -\frac{1}{\rho r}\frac{\partial p}{\partial\varphi} - 2\Omega u\sin\varphi + \frac{1}{\rho}\frac{\partial\tau_\varphi}{\partial r} \qquad (0.8)$$

$$\frac{dw}{dt} - \frac{u^2 + v^2}{r} = -\frac{1}{\rho}\frac{\partial p}{\partial r} - g + 2\Omega u\cos\varphi$$

To simplify the above equation the following steps can be taken. Using the shallow approximation, which states that $z \ll a$, i.e. the atmosphere is a thin layer residing on the earth, and using scale analysis, the w terms can be considered much smaller than u and v and can be removed from the first two equations in (0.8). Likewise the u and v terms can be removed from the third equation in (0.8). The frictional contribution can be represented by $\mathbf{F}$ and $2\Omega\sin\varphi$ is the Coriolis parameter f. The second terms of the first two equations can be removed by assuming a local tangent plane is being used. This approximation applies whenever the horizontal scale is much smaller than the radius of the earth. The final equations of motion become

$$\frac{Du}{Dt} = -\frac{1}{\rho}\frac{\partial p}{\partial x} + fv + \mathbf{F}_x$$

$$\frac{Dv}{Dt} = -\frac{1}{\rho}\frac{\partial p}{\partial y} - fu + \mathbf{F}_y \qquad\qquad (0.9)$$

$$\frac{Dw}{Dt} = -g - \frac{1}{\rho}\frac{\partial p}{\partial r}$$

This completes the derivation of the fundamental equation for the conservation of momentum introduced in the beginning of the section. Equations (0.9) are referred to as the equations of motion for the atmosphere on a local plane.

c.   The Continuity Equation

In the next conservation law, consider the mass contained in some unit volume $\delta V = \delta x \delta y \delta z$. We can again represent the introduction of mass on the left side of a cube as a truncated Taylor series as shown in Fig 4. The amount of mass leaving the cube on the right side is also represented. The change in the mass from some component of velocity in the x direction is
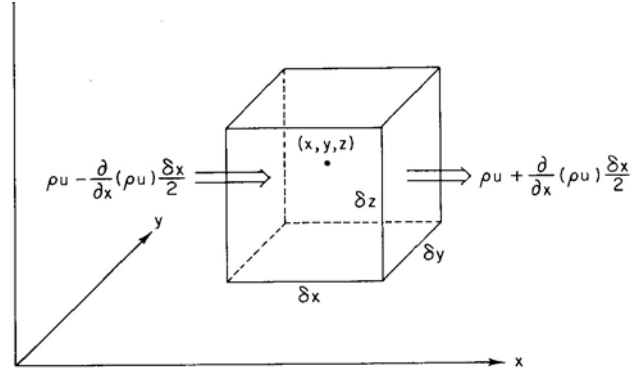
Figure 4   Showing the Transport of Mass through a Unit Volume. (*From Holtonyear*)

$$\left[\rho u - \frac{\partial}{\partial x}(\rho u)\frac{\delta x}{2}\right]\delta y \delta z - \left[\rho u + \frac{\partial}{\partial x}(\rho u)\frac{\delta x}{2}\right]\delta y \delta z = -\frac{\partial}{\partial x}(\rho u)\delta x \delta y \delta z$$

so that the total flow of mass from all three directions becomes

$$-\left[\frac{\partial}{\partial x}(\rho u) + \frac{\partial}{\partial y}(\rho v) + \frac{\partial}{\partial z}(\rho w)\right]\delta x \delta y \delta z$$

10

and the mass inflow per unit volume is $-\nabla\cdot(\rho\mathbf{U})$. Since mass cannot be created nor destroyed within the volume, any change to the density of the volume ($\frac{\delta\rho}{\delta t}$) would be due to the net flux of mass of the box.

$$\frac{\delta\rho}{\delta t}+\nabla\cdot(\rho\mathbf{U})=0 \tag{0.10}$$

or,

$$\frac{\delta\rho}{\delta t}+\rho\nabla\cdot\mathbf{U}+\mathbf{U}\cdot\nabla\rho=0$$

or, if the first two terms are combined,

$$\frac{D\rho}{Dt}+\rho\nabla\cdot\mathbf{U}=0 \tag{0.11}$$

Equation (0.10) differs from equation (0.11) in that the first equation gives the local rate of change of the density and the mass divergence and the second equation gives the absolute change in the density of a parcel of air following the motion of the air parcel.

By applying a synoptic scale analysis to the above continuity equations, a simplified form can be used. Equation (0.11) becomes

$$\frac{\partial\rho}{\partial t}+u\frac{\partial\rho}{\partial x}+v\frac{\partial\rho}{\partial y}+w\frac{\partial\rho}{\partial z}+\rho\left(\frac{\partial u}{\partial x}+\frac{\partial v}{\partial y}+\frac{\partial w}{\partial z}\right)=0$$

The density parameter ρ can be approximated by the quantity $\rho_0+\rho'$ where ρ_0 is the average density of the volume and ρ' is the deviation from the average. In this way, time differentiation of the average density term will be zero.

$$\underbrace{\underbrace{\frac{\partial\rho'}{\partial t}+u\frac{\partial\rho'}{\partial x}+v\frac{\partial\rho'}{\partial y}}_{\sim\frac{U}{L}\delta\rho}+\underbrace{w\frac{\partial\rho'}{\partial z}}_{\sim\frac{W}{D}\delta\rho}+\underbrace{w\frac{\partial\rho_o}{\partial z}}_{\sim\frac{W}{H}\delta\rho}}_{A}+\underbrace{(\rho_0+\rho')}_{\rho_o+\rho'}(\underbrace{\frac{\partial u}{\partial x}+\frac{\partial v}{\partial y}}_{\sim\frac{U}{L}}+\underbrace{\frac{\partial w}{\partial z}}_{\sim\frac{W}{D}})=0 \tag{0.12}$$

11

Here, the synoptic scales used are

L	Horizontal length scale
H	Vertical length scale
D	Vertical length scale of disturbance
U	Horizontal scale for advection
W	Vertical scale for advection

In the case of a compressible fluid such as the atmosphere the following approximations can be made. The density disturbance term $\delta\rho$ is much smaller than the average density of the fluid ρ_0. Given that, term A in equation (0.12) is much smaller than term (E)(F) and can be removed. Term B is much smaller than term (D)(G) and can be removed. Finally, term E is much smaller than term D and can also be removed. Equation (0.12) is simplified to

$$w\frac{\partial\rho_0}{\partial z}+\rho_0\nabla\bullet\mathbf{v} \qquad\qquad (0.13)$$

This equation will take on different forms depending on whether the atmospheric fluid under consideration is non-hydrostatic as in the COAMPS model (see section 3 below) or hydrostatic such as the NOGAPS model (see section 2 below) where the first term in equation (0.13) can be ignored.

d.   The Thermodynamic Equation

The law of conservation of energy states that the energy added to a system is equal to the change in internal energy of the system plus the work done by the system. In the atmospheric air parcel case the internal energy is due to the kinetic interactions of molecules within the control volume. Work is done when the boundaries of the control volume is changed. The work performed on the control volume originates from the external forces described above and acting on the surface area of the control volume.

12

The thermodynamic energy of a control volume can be represented in a Lagrangian system as $\rho[e+\dfrac{\mathbf{U}\cdot\mathbf{U}}{2}]\delta V$ where e represents the internal energy per unit mass and $\mathbf{U}$ is the velocity of the control volume system. This second term represents the kinetic energy of the system. The pressure force acts on the entire surface of the control volume. The rate at which the pressure force does work on the control volume is the dot product of the force per unit area and the velocity vector. Hence, the rate at which the environment does work on a unit volume in the x direction is

$$(pu)_A\delta y\delta z-(pu)_B\delta y\delta z.$$

In this infinitesimal control volume the work performed on side A is nearly equal to the work performed on side B. Therefore

$$(pu)_B=(pu)_A+\left[\frac{\delta}{\delta x}(pu)\right]_A\delta x+\cdots$$

and the net rate at which pressure does work on the control volume in the x direction can be approximated by

$$\left[(pu)_A-(pu)_B\right]\delta y\delta z=-\left[\frac{\delta}{\delta x}(pu)\right]_A\delta V.$$

Similar expressions can be found for the y and z directions. The total rate at which pressure does work on the control volume becomes

$$-\nabla\bullet(p\mathbf{U})\delta V.$$

As discussed earlier, the frictional force acts perpendicular to the velocity vector and therefore does not contribute to the work performed on the control volume. Likewise, the Coriolis force, $-\Omega\times\mathbf{U}$, is perpendicular to the velocity and also does not contribute to the work. The gravity force $\mathbf{g}$ can be dotted with the velocity vector $\mathbf{U}$ when directed downward. Summing all contributions the conservation of energy equation, when applied to a control volume in the Lagrangian system, becomes

$$\frac{D}{Dt}\left[\rho\left(e+\frac{\mathbf{U}\cdot\mathbf{U}}{2}\right)\right]=-\nabla\bullet\left(p\mathbf{U}\right)\delta V+\rho\mathbf{g}\bullet\mathbf{U}\delta V+\rho J\delta V \tag{0.14}$$

Here J is the rate of heating per unit mass owing to radiation, conduction, and latent heat release. The last term in equation (0.14) represents the contribution to the internal energy from radiation and latent heat release. Using the chain rule (0.14) becomes

$$\rho\delta V\frac{D}{Dt}\left(e+\frac{\mathbf{U}\cdot\mathbf{U}}{2}\right)+\left(e+\frac{\mathbf{U}\cdot\mathbf{U}}{2}\right)\frac{D\left(\rho\delta V\right)}{Dt}=-\mathbf{U}\bullet\nabla p\delta V-p\nabla\bullet\mathbf{U}\delta V-\rho gw\delta V+\rho J\delta V \tag{0.15}$$

where $\mathbf{g}$ in equation (0.14) only acts parallel to the z component of the velocity. From the Lagrangian form of the continuity equation $\frac{D}{Dt}\left(\rho\delta V\right)=0$ and the second term on the left hand side of (0.15) is equal to zero. Thus

$$\rho\frac{De}{Dt}+\frac{D}{Dt}\left(\frac{1}{2}\mathbf{U}\cdot\mathbf{U}\right)=-\mathbf{U}\bullet\nabla p-p\nabla\bullet\mathbf{U}-\rho gw+\rho J \tag{0.16}$$

Using the Lagrangian form of the momentum relation above in equation (0.7) without friction, the following relation

$$\rho\frac{D}{Dt}\left(\frac{1}{2}\mathbf{U}\cdot\mathbf{U}\right)=-\mathbf{U}\bullet\nabla p-\rho gw \tag{0.17}$$

can be used to simplify (0.16) to

$$\rho\frac{De}{Dt}=-p\nabla\bullet\mathbf{U}+\rho J \tag{0.18}$$

The thermal energy equation of (0.18) can be written in more familiar form by noting from (0.11) that

$$\frac{1}{\rho}\nabla\bullet\mathbf{U}=-\frac{1}{\rho^2}\frac{D\rho}{Dt}=\frac{D\alpha}{Dt}$$

and that for dry air the internal energy per unit mass is given by $e=c_\upsilon T$, where c_υ is the specific heat at constant volume. Here $\alpha=1/\rho$ and is called the specific volume. Now the familiar form of the thermodynamic equation becomes

14

$$c_\upsilon \frac{DT}{Dt} + p \frac{D\alpha}{Dt} = J \qquad\qquad (0.19)$$

The above fundamental equations along with the ideal gas law can be grouped together to form a complete set of equations to describe the fluid motion of the atmosphere. Computational models can use these equations to aid in forecasting and in understanding how atmospheric flows occur.

2. A Brief Discussion on the Navy Operational Global Atmospheric Prediction System (NOGAPS)

In the NOGAPS model (*Hogan and Rosmond, 1991*), generated by Naval Research Laboratories (NRL)-Monterey, the Navy uses the primitive equations to construct a spectral global atmospheric weather prediction system. The NOGAPS model equations are provided in Appendix B. This model is important in providing guidance for world-wide naval operations and providing the forcing and boundary conditions for a number of atmospheric and oceanographic application programs. NOGAPS provides the real data initial conditions required to set up the first guess fields that represent the initial state of the atmosphere in the Coupled Ocean/Atmosphere Mesoscale Prediction System (COAMPS), the mesoscale atmospheric model of the United States Navy. In the COAMPS model (*Hodur, 1997*), this is referred to as a 'NOGAPS cold start' and is one of the two methods to initiate a COAMPS real data model forecast.

NOGAPS version 4.0 was released in 1998 and contains 239 spectral waves with a 0.5-degree resolution. There are 30 sigma levels with approximately six levels below 850 mb, depending on the terrain. NOGAPS utilizes a hybrid pressure coordinate system. The numerical method in NOGAPS uses a horizontal spectral differencing, second-order finite difference in the vertical, and central time differencing with Robert semi- implicit corrections. Additional information on NOGAPS can be found in *Hogan and Rosmond (1991).*

3. The Basics of the Coupled Ocean/Atmosphere Mesoscale Prediction System

COAMPS was implemented at the Fleet Numerical Meteorological Oceanographic Center (FNMOC) in October of 1997. COAMPS provides the Navy with a "finer-scale" meteorological representation of the atmosphere by decreasing the grid size of the model and introducing additional physics that can be handled on a local scale that otherwise could not on the NOGAPS global scale model. Numerically, the model uses the primitive equations and includes nonhydrostatic effects on an Arakawa C grid. The model equations used for COAMPS are provided in Appendix C.

a. Grid Structure

The Arakawa C grid was chosen due to its better performance regarding geostrophic adjustment and divergent flow. The grid consists of the momentum components (u,v,w) shifted one-half grid interval from the location of the other prognostic variables. The grid is staggered in both the horizontal and vertical direction. There are thirty sigma levels in the vertical in the current operational configuration. A horizontal depiction of the Arakawa C grid is shown below for the prognostic variable π, the dimensionless pressure.

$$\pi_{i-1,j+1} \quad u_{i-1,j+1} \quad \pi_{i,j+1} \quad u_{i,j+1} \quad \pi_{i+1,j+1}$$
$$v_{i-1,j} \qquad\qquad v_{i,j} \qquad\qquad v_{i+1,j}$$
$$\pi_{i-1,j} \quad u_{i-1,j} \quad \pi_{i,j} \quad u_{i,j} \quad \pi_{i+1,j}$$
$$v_{i-1,j-1} \qquad\qquad v_{i,j-1} \qquad\qquad v_{i+1,j-1}$$
$$\pi_{i-1,j-1} \quad u_{i-1,j-1} \quad \pi_{i,j-1} \quad u_{i,j-1} \quad \pi_{i+1,j-1}$$

b. COAMPS Nested Domains

The COAMPS model can be run with up to seven horizontally nested grids. The resolution of each inner consecutive nest is increased by a factor of three. Every third grid in the inner nest corresponds to a grid point in the outer nest. The outer grid is also called the coarse nest for the parent/child nest pairing. The inner nest can also be called the fine nest. The current operational grid sizes used at FNMOC are 81, 27 and 9 km grid spacing. Higher resolution combinations can also be used. FNMOC will soon be increasing the operational grid spacing to 54, 18, and 6 km. The latter combination

was the grid spacing used in this study. COAMPS provides for one-way and two-way interactions between the coarse and fine grid.

c.   COAMPS Integration Scheme

COAMPS uses second-order leapfrog time differencing to integrate the slow modes (advective solution) using a time step Δt that depends on the grid resolution and advective speeds to ensure computational stability.   Because COAMPS is nonhydrostatic, the simulations also contain sound and gravity wave solutions. Their faster propagation rates require integrations over a smaller forward time step, and are designated by the number of fast time steps per slow time step. Semi-implicit vertical differencing and the use of quasi-compressible assumptions allow COAMPS to increase the number of fast time steps such that the speed of sound can be much less than its typical atmospheric value of ~350 m/s.

d.   Initial Guess Field

The initial guess field comes either from the NOGAPS model (known as a 'NOGAPS cold start') or from the previous COAMPS forecast field. For the NOGAPS cold starts, global fields for the pressure levels at 0.5 degree resolution are interpolated to the COAMPS model grid points. The current boundary conditions are derived from the *Davies (1976)* or *Perkey-Kreitzberg (1976)* treatment of NOGAPS forecast fields at 3-hour intervals and will be discussed in greater detail below. Additional information on COAMPS can be obtained from *Hodur (1997).*

B.   CURRENT TREATMENT OF MODEL LATERAL BOUNDARY CONDITIONS

1.   The Lateral Boundary Condition Problem

Regional models require higher resolution grids and additional physical parameterizations in order to better define the atmospheric flow. In turn, the larger grids and parameterization requires increased computational time and inhibits the ability to perform such a model on the global scale given operational time constraints. This limitation necessitates that regional models have lateral boundary around their perimeter.

The regional model resides within a global model such as NOGAPS. The conditions along the perimeter of the regional model are derived from the global model.

Differences between the two models can lead to erroneous solutions within the regional model. The higher resolution of the inner model requires that the global model grid point data be interpolated to provide data to the unmatched inner grid points along the boundary. In effect, the interpolation is generating mesoscale data where previously there was none. This could lead to erroneous data propagating within the regional model. Another problem is the possible inconsistent handling of physical parametric processes between the global and region models. Different methods of parameterization, such as cumulus convection, can lead to erroneous gradients in the boundary region in which error will propagate *(Warner et al. 1997)*. Temporal resolution can also be a problem. COAMPS uses the 12 hour NOGAPS forecast to generate the COAMPS coarse nest lateral boundary conditions. Although the 12 hour forecast is generally considered quite good *(FNMOC, 2004)*, small discrepancies can cause errors to propagate through the model.

Proper handling of the lateral boundary conditions is required to limit the propagation of errors through regional models. The most recent NOGAPS forecast is used to generate the COAMPS outer nest lateral boundary condition for a real data simulation. The NOGAPS fields are horizontally interpolated using a bicubic spline to the COAMPS coarse grid, then interpolated in the vertical to the model vertical coordinates. COAMPS can either use the *Perkey-Kreitzberg (1976),* which specifies the boundaries according to the NOGAPS tendencies, or the *Davies (1976)* method, which uses the actual NOGAPS fields to determine the lateral boundary conditions.

a.   *Perkey-Kreitzberg Method*

In the Perkey-Kreitzberg method, the boundary conditions consist of large-scale time-varying tendencies provided by the global model linearly combined with model-calculated tendencies. The prediction of any dependent variable χ can be written as:

$$\chi_n(I) = \chi_p(I) + W(I)\frac{\partial \chi_m}{\partial t}\bigg|_I \Delta t + [1 - W(I)]\frac{\partial \chi_{ls}}{\partial t}\bigg|_I \Delta t \quad (0.20)$$

where the subscripts *n* and *p* denote the "new" value after the boundary condition and the "previous" value at a former time. The *ls* denotes the large-scale specified tendency of χ, and *m*, the model-calculated tendency. The values of the weighting coefficients *W* are constructed such that the interior grid points are of value unity, the boundary grid points are zero, and there is a transition "buffer" layer between the two. In COAMPS, the transition is seven grid points wide. Thus, the outer grid points of the LAM are completely determined by the global model, the interior points are derived from the regional model, and there is a limited transition zone between the two.

The Perkey-Kreitzberg model has a tendency to transfer the energy of interior generated long waves to the short wave region *(Perkey and Kreitzberg, 1976)*. The energetic short waves are reduced by introducing a period filter in the boundary region. In their paper, Perkey and Kreitzberg demonstrate that an exterior generated wave will propagate through a regional model with little deformation. Interior waves generated by physical processes within the model will dissipate within the transition zone, effectively "leaving" the model region with little reflection at the boundary. This method proved to be an effective way to handle the boundary problem between global and regional models.

b.   Davies Method

The Davies approach is to construct a boundary formulation that is consonant with the governing equations but also alleviates the effect of the inaccurate boundary data. In this way, alternate governing equations are used that reduce the sensitivity to boundary conditions and reduce the generation of noise on the boundary. For example, in the case of a linear, inviscid, compressible flow confined between two boundaries (flow is independent in the *y*-direction), the governing equations can be written as:

$$u_t + Uu_x + w_z U - fv = -p_x - K(u - \tilde{u}) \quad\quad (0.21)$$

$$v_t + Uv_x + f(u+U) = E - K(v-\tilde{v}) + F[v-\tilde{v}] \qquad (0.22)$$

$$p_t + Up_x + c^2 u_x = -c^2(w_z + wS) - K(p-\tilde{p}). \qquad (0.23)$$

Here, E ($E=fU$) is the external forcing, and the function K and the functional F contain the mathematical treatment of the boundary conditions. The mean flow is U and an estimate of the time development of the flow field in the neighborhood of the boundary is denoted by the over barred fields $\tilde{u}$, $\tilde{v}$, $\tilde{p}$. The specified function $K = K(x) \geq 0$ is continuous and non-zero only in the vicinity of the boundary. The functional F is defined by $F[v-\tilde{v}] = \int_L^x K_x(v-\tilde{v})dx$. In effect, K and F act to reduce the prognostic variables near the boundary that are different than the prescribed values generated from the global model. The relaxation coefficients smooth the fields in the location of the boundary.

For the Davies methodology, the K term acts as the weighting functions much like the W term discussed above for the Perkey-Kreitzberg. The difference is how the weighting factors are used. For the Perkey-Kreitzberg, as can be seen in equation 1.20, the new prediction for the dependent variable within the boundary zone is determined by a time integrated transition of the outer model to the inner model. The Davies model uses the boundary zone weighting functions within the governing equations, which include both time *and* spatial dependent variables. The Davies technique implements the boundary correction while solving the governing equations. The Perkey-Kreitzberg technique implements the boundary correction after solving each time step of the governing equations.

Although either the Perkey-Kreitzberg or the Davies boundary treatment can be selected in COAMPS, the Davies method is the only one that has been rigorously tested by NRL – Monterey, and used operationally at FNMOC *(Doyle, 2004)*.

II. THE EXPERIMENT

A. EXPERIMENT SET UP

To analyze the effect of the lateral boundary on the inner nest of a COAMPS forecast, the following experiment was constructed. Four sets of COAMPS forecast data runs were performed. The coarse and fine domain of the control run corresponded to the first and second nest of the COAMPS European Operational Area run at FNMOC. The coarse grid for the remaining three test runs expanded geographically to the west and the north of the control run coarse grid. The fine grid for the three test runs had roughly the same geographical position as the control run fine grid. The latitude and longitude grid points did not match up exactly for all runs. This slight difference in grid point positioning will be discussed in more detail below. The inner and outer domain boundaries can be seen in Figure 5.

Research on the COAMPS lateral boundaries was performed in conjunction with efforts at FNMOC to study methods to improve operational handling of the lateral boundaries. Data for this analysis was acquired from FNMOCs project, "COAMPS Operational Configuration Testing". A copy of the FNMOC proposal is provided in Appendix D. FNMOC research was conducted over a three month period from 15 December 2003 until 15 March 2004. COAMPS forecasts carried out by FNMOC extended to 48 hours. For this study, a request was granted to extend the forecast fields out to 144 hours by rerunning the forecasts using the COAMPS restart data fields for the selected model dates of interest.

Two forecast periods of interest were chosen. The study set consisted of the COAMPS Analysis and the following 144 hours of forecast fields at six hour intervals. Time periods containing an "active" and an "inactive" period were chosen for study. Time periods were chosen based on the strength of the 300 mb jet running zonally through the upwind portion of the FNMOC European Operational Area. The active time period contained a strong jet located on the upwind side of the European Operational Area for a six day period based on twelve hour NOGAPS Analysis fields (see Figure 6 in

21

Appendix A). The model run chosen for the active period was 07 January 2004, 0000 UTC. For the inactive period, no sustained zonal jet was present within the FNMOC European Operational Area (see Figure 7 in Appendix A). The model run chosen for the inactive period was 04 March 2004, 0000 UTC.

For the time periods stated, four sets of COAMPS model runs were performed. Each run consisted of an inner fine nest at 18 km resolution with the same given geographical location. Each had a coarse outer grid nest at 54 km resolution, with an expanding geographical location. The control data run is identical with the inner and outer grids used by FNMOC for the operational European grid. The control model run will also be identified as Run1. The remaining model runs were identified as Run3a, Run3b and Run3c. Run3c had the largest coarse grid and Run3a had the coarse grid closest to the control outer grid. The geographical locations for each outer grid
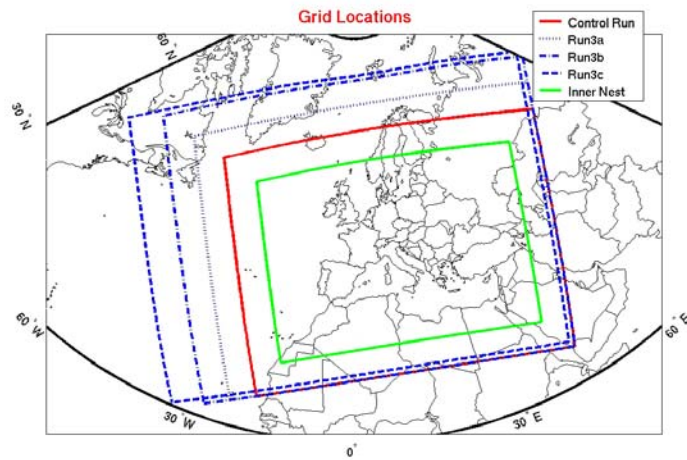
Figure 5   Grid Locations for the Inner and Outer Grids for Run1, Run3a, Run3b and Run3c. Inner grid for all four runs shown in green. Outer grid for control run shown in red. Outer grid for Run3a/b/c shown as dotted, dot-dashed and dashed respectively.

are shown in Figure 5. A spread sheet containing model set up information derived from the COAMPS datahd fields are provided in Appendix E. The datahd file is the file generated from the COAMPS Analysis program that indicates the domain configuration and program settings used in the particular run.

1.   Data Field Mismatch

The boundary locations for the coarse grids shown in Figure 5 were determined from the outer grid points of the latitude and longitude fields from the COAMPS runs. The values contained in the lat/long fields correspond to the locations of the data

contained in the COAMPS data fields. As can be seen in Figure 5, information for Run3c has been shifted toward the northwest compared to the other three data runs. As a consequence, the inner grid for Run3c has also been shifted (not shown in Figure 5). The mismatch was caused by the improper setup of the Run3c domain.

To get the most accurate comparison of data points, the grid points used in the study were compared based on their geographical locations, and not necessarily grid point number. The only shift required was for Run3c. In effect, the top six rows of horizontal data points of Run3c and the bottom six rows of horizontal data points of Run1/3a/3b were not included for comparison. As listed in Appendix E, this reduced the number of north/south grid points from 196 to 191. The total reduction in data points from 57,820 to 56,345 reduces the amount of analyzed data by 2.55%.

After the readjustment of grid points for data field comparisons, the maximum deviation between the control run latitude/longitude grid points and the latitude/longitude points associated with the data runs for Run3a/b/c was determined to be small enough to allow for sufficient comparison. The maximum deviations in degrees and in kilometers are listed in Table 1 below.

	Run3a		Run3b		Run3c	
Max lat deviation	0.0020°	0.22 km	0.0082°	0.90 km	0.0032°	0.35 km
Max long deviation	0.0057°	0.63 km	0.0121°	1.33 km	0.0059°	0.65 km

Table 1   Max Lat/Lon Deviation

2.   Comparison Method

To get a visual picture of how the separation distance between the coarse grid and the fine grid lateral boundaries change the forecast outcome, contours of each data run were plotted on the same figure. The contour lines had the following coloring convention; red for the control run, blue for Run3a, green for Run3b and magenta for Run3c. To determine whether differences in the contour lines were significant, the following method was used. The standard deviation for each forecast hour of the control

run was calculated using MATLAB. Then MATLAB was used to determine how the test runs differed from the control run. The control run field was subtracted from the test run field point for point over the entire inner nest domain. Then the root mean square (RMS) difference of the comparison field was calculated. If the RMS difference of the comparison field was below the standard deviation of the control field alone, then it was assumed that the differences observed in the contour fields were within the level of natural variation of the control field, and therefore insignificant. As will be shown, it proved sufficient to compare the RMS differences with the minimum standard deviation of the control field.

Run1, with the smallest outer domain, was used as the control instead of Run3c with the largest outer domain, as typically would have been done. It is assumed that the run with the largest outer boundary will have the least adverse effects from the boundary and therefore be the closest to the true solution *(Warner et al, 1997)*. Since this work was performed in conjunction with FNMOC research, and in their research Run1 was used as the control (see Appendix D), the same convention was used here. As a consequence, computed differences between the control (Run1) and the test runs (Run3a/b/c) will appear to increase more quickly for the largest outermost domain, and more slowly for the smallest outermost domain.

A smaller outer domain would mean the outer and inner boundaries are closer together. This would imply that adverse boundary effect would populate the inner domain more quickly and grow larger than for a model run where the outer domain was larger. Here, the comparison is performed with the model run with the smallest outer domain, or the one least likely to be correct when compared to truth. Since Run3c has the largest outer domain and is most likely to be correct when compared to truth, its RMS differences grow the fastest when compared to Run1, the control.

B. ANALYSIS OF RESULTS

1. Active Period

Figure 8 in Appendix A shows the sea level pressure contour lines for the active periods. The figure includes the COAMPS forecasts in 24 hour increments out to 144 hours. The 24 hour forecast sea level pressure fields were missing from the FNMOC data set, and therefore were not included in the analysis. The contour lines depicted are the 980, 1000 and 1020 mb contours.

For the SLP COAMPS Analysis ('000' forecast hour) in the upper left corner of Figure 8, the contour lines appear to nearly coincide, although there are slight differences. The 1020 mb contour located off the coast of Portugal splits into two groups. Contour lines for Run1 and Run3a follow a Northeast-Southwest direction, and then cut in to an East-West direction before rejoining the other two test run contours. The same contours for test runs 3b and 3c maintain a North-South orientation in the same general location. Since all runs had the same settings and input parameters, slight variations in the contour lines such as these are solely due to the geographical placement of the outer grid. Slight variations in the COAMPS Analysis occur solely due to the geographic configuration of the grid domain.

In Figure 9, a horizontal depiction of the difference between the control and Run3c for the COAMPS Analysis, '000' forecast for the active time period can be seen. In Figure 9, blue areas represent areas where the test run sea level pressure is below the control run sea level pressure. Yellow/red areas represent areas where the test run pressure is greater than the control run. Control run contour lines have been added for reference. As can be seen by the colorbar in Figure 9, the difference between test Run3c and the control run is slight. There are differences between the control and the test run COAMPS Analysis that are solely due to the geographical domain set up, but these differences are slight, and have little effect on the sea level pressure contour lines.

As the COAMPS forecast progresses, the variability in the SLP contour lines increase as can be seen in Figures 8. For the active period the variability is greatest in the northwest region at the 120 forecast hour. Again, looking at the horizontal difference

depictions between the control run and Run3c for the active period, variations can be seen. The 120 and 144 SLP fields are shown in Figures 10 and 11 respectively. Variations of up to 20 mb differences can be seen between the control run and Run3c.

In Figure 12, the standard deviation of the control run is plotted over the forecast period for both the active and the inactive period. The minimum standard deviation for the active period occurred just prior to the 72 hour forecast and reached 10.6 mb. The minimum standard deviation for the inactive period occurred at the 90 hour forecast and reached 6.1 mb.

In Figures 13, the minimum standard deviations were compared to the RMS differences between the control run and the individual test runs. The maximum RMS differences occurring at the end of the forecast period are far below that of the standard deviation of the control run. For the active time period in Figure 13, the maximum RMS was about 5.5 mb, which is approximately half the value of the minimum control run standard deviation. So when the entire grid domain is under consideration, the differences observed between the test runs and the control run are within the natural variability of the control run alone.

As can be seen in Figures 10 and 11, there are isolated areas where the SLP difference between the control and Run3c are as large as 20 mb. For forecasting purposes a 20 mb error could mean the difference of predicting an active cyclone or not. For instance, in Figure 11 the control run predicts a 980 mb pressure low over central Europe. In the same location, Run3c predicts a pressure of 15 to 20 mb greater, equivalent to the surrounding area and therefore no low pressure system was predicted. Similarly, on the northwest edge of the domain, Run3c predicts the 980 mb contour to be much more extensive than the control. The control run closes the 980 mb contour with the edge of the domain to the northeast of the British Island whereas Run3c extends the 980 mb contour farther west.

Even though differences between the test runs and the control were found to be minimal when the entire domain was considered, there were isolated areas where significant differences occur. From a forecaster's perspective, the "interesting" weather

26

observed at the surface is forced by the presence of a low pressure system. As the cyclonic motion wraps around and into the low pressure system, high winds develop at the surface. Higher winds drive the surface wave heights. For a naval vessel, high seas and winds can cause, at best, uncomfortable living conditions onboard ship and, at worst, disastrous damage to ship and crew. To avoid adverse weather conditions, naval vessels rely on weather forecasters to predict the location and strength of low pressure systems. At times, operational restraints require naval vessels to traverse in close proximity to low pressure systems, so accurate and timely forecasts are a must. Operational commanders require the most accurate information, including weather information, to plan effectively. Differences in forecasted cyclonic positioning and strength due to differences in model setups could change the operational effectiveness of the naval vessel.

To see where the domain size begins to affect the predicted outcome of the forecast, a subset of the domain grid points was used. The forecaster is concerned with low pressure systems, therefore for the active case, the subset of domain points below the 990 mb pressure level was considered for reevaluation. The same method of comparing the STD of the control with the RMS of each run was used to reevaluate the 990 mb subset. Here, the total number of points changed with each forecast time step, since the 990 mb contour changes with each time step. Also, all four data runs were used to determine the subset of data points used to calculate the STD and RMS values at each time step.

Figure 14 shows the STD and RMS values from the active period sea level pressure below 990 mb. The STD of the control run is in red. The RMS difference between the control run and Run3a/b/c are given in blue, green and magenta, respectively. Below Figure 14 is a table stating the percentage of domain points having a sea level pressure below 990 mb. The percentage was determined after the correction was made for the domain mismatch discussed in the previous section. By the 72 hour forecast, the control run STD fell to half its initial value and the RMS values began to increase. At the 78 hour forecast, Run3c RMS values exceed the control run STD.

27

The Petterssen Development Equation can be used as a model of the development of synoptic scale extra-tropical low pressure systems. It can be expressed as

$$\left(\frac{\partial \varsigma}{\partial t}\right)_{P_0} = \left[-\mathbf{v_g} \cdot \nabla_p \eta\right]_{500} - \frac{g}{f}\nabla_p^2\left(-\mathbf{v_{g_0}} \cdot \nabla_p\left(Z_{500} - Z_{1000}\right) + \bar{\sigma}\omega + \frac{\bar{\dot{Q}}}{c_p\rho}\right)$$

where the left hand side represents the change in the geostrophic vorticity at the surface. If $\left(\frac{\partial \varsigma}{\partial t}\right)_{P_0} > 0$, cyclogenesis is occurring and a low pressure system initiates and/or strengthens. If $\left(\frac{\partial \varsigma}{\partial t}\right)_{P_0} < 0$, cyclolysis is occurring and a low pressure system fills or is inhibited. The first term on the right hand side represents the advection of vorticity at the level of non-divergence. Positive vorticity advection (PVA) at the level of nondivergense contributes to cyclogenesis by promoting cyclonic motion within the air column and inducing vertical motion. The second term on the right hand side represents the thermal advection. By making simplifying assumptions the warm air advection can be represented as a sine wave. After the assumptions have been made, the Petterssen Development Equation predicts that warm air advection contributes to cyclogenesis. The third term is the braking term which inhibits development by cooling the column due to adiabatic cooling of rising air. The last expression on the right hand side is the diabatic heating term. The two major development terms are the vorticity advection and thermal advection. A closer study of these two terms was performed to get a sense of how the COAMPS outer boundary impacts cyclonic development using the Petterssen Development Equation.

a.   Case 1

The 84 hour forecast of the thermal advection is shown in Figure 15 for the active period. The SLP for the equivalent time period is shown in Figure 16, as well as the 6 hour prior forecast. As can be seen, there is a large area of positive thermal advection over Central Europe. The fact that this advection is stronger for the control run, seen as a deeper shape of yellow, may be contributing to the forecasted small low

28

pressure system for the control run, seen as the 1000 mb contour over the Czech Republic, that is not present for Run3c, seen as a yellow area in Figure 16 over the same location.

b.   Case 2

In the 96 hour forecast, large areas of vorticity advection for the control run active period can be seen in Figure 17. In Figure 17, areas of positive vorticity advection (PVA) are shaded yellow/red.   No substantial PVA or negative vorticity advection (NVA) was present in the 6 hour forecasts prior to and following the 96 hour forecast (figures not shown.) One area of PVA in the 96 hour forecast is associated with the 500 mb trough extending over the Mediterranean Sea. The influence of the PVA can be seen in the sea level pressure forecasts in Figures 18 and 19. Figures 18 and 19 shows the progression of the SLP from the 90 hour forecast to the 108 hour forecast. At the 90 hour frame, a previously developed relative low pressure system resides of the country of Greece. By the 96 hour forecast, the low pressure system deepened in the control run seen as an expansion of the 1000 mb contour line. For the next 12 hours, after the PVA has expired, there was no further deepening of the low pressure system. In contrast, the low pressure system for Run3c begins to fill between the 90 and 96 hour forecast. This can be seen as a progression from blue shading, indicating the test field below the control field, to yellow shading, indicating the test field above the control field. By the 108 hour forecast it appears the control run low pressure system extends from the Aegean Sea up into Romania. The low pressure system for Run3c has completely filled over the Aegean Sea, and has moved exclusively over the European Continent over Ukraine.

2.   Inactive Period

The comparison all four COAMPS Analysis ('000' forecast) runs is show in Figure 20 for the inactive period. Like the active period seen in Figure 8, the contour lines are closely packed, only indicating slight differences between the four runs. The largest difference seen in Figure 20 is the cut off 1020 mb low over the Atlantic. Figure 21 shows the horizontal depiction of the difference between the control run with the smallest outer domain and Run3c with the largest outer domain. Here the two fields agree to within 2 mb over the entire inner nest domain.

29

As the forecast progresses, the contour lines begin to separate as can be seen in Figure 20. Like the active period, the largest contour spreads seem to occur over the Atlantic at the upwind side of the inner nest domain. There is also a large disagreement by the 120 hour forecast on the position and extent of the 1020 mb relative low pressure system in center of the model domain. The smaller outer grid domains of Run3a and the control maintain the 1020 mb system over the Mediterranean Sea whereas the larger outer grid domains of Run3b and Run3c extend the 1020 mb contour up into lower Europe. Figure 22 shows the horizontal depiction of the numerical difference between the sea level pressures of the two extreme cases of outer domain size. The darkened blue area over Ukraine signifies that Run3c SLP was below the control run in this area. The yellow/red area over the 1020 mb control run contour indicates that the SLP was much higher in this region for Run3c. The low pressure system for Run3c was shifted further to the northeast of the control run low pressure system.

As with the active period, a comparison was made of the RMS difference between the test runs and the control run, and the standard deviation of the control run alone. Figure 23 shows that the RMS differences during the inactive period were below the minimum value of the control run standard deviation. The minimum standard deviation of the control run during the inactive period was smaller than the minimum standard deviation of the control run during the active period. Therefore the maximum RMS differences were closer to the minimum standard deviation of the control run. Still, this shows that when the entire inner domain field is considered, the differences observed in the test runs are within the natural variability of the control run, and are therefore insignificant.

Like the active period, there are locations within the domain were deviations are large and exceed the level of natural variability of the control run. Again, taking the forecasters perspective, forecasted differences of low pressure systems can drastically change operational priorities for the U.S. Navy. Using the same analysis discussed in the active section, the SLP contour below which RMS differences exceed the control run standard deviation was found to be 1010 mb, as seen in Figure 24. In the 1010 mb subset

of domain grid points shown in Figure 24, the standard deviation of the control run was only 3 mb and the RMS differences of the test runs exceed this value around 96 hours. By 144 hours, the RMS differences are approximately the same value as the control maximum standard deviation value. At this point the differences between the model runs become significant.

The Petterssen Development Equation was again used to see how differences in the upper atmosphere changed the level of surface cyclonic development.

a. Case 3

Figure 25 shows the advection of relative vorticity for the inactive period at the 54 hour forecast. In it, there is a large area of PVA in the northern Mediterranean between Spain and Italy that is much stronger for the control run than for Run3c. The influence of this PVA can be seen in the SLP depiction. Figure 26 shows the 6 hour prior SLP and the SLP for the concurrent time as the PVA. Initially, Run3c pressure contour was only slightly above the control run pressure, seen as a slight yellowing over the northern Mediterranean. As the PVA develops above the area, a low pressure system begins to initiate for the control run, seen as the addition of the 1000 mb contour in Figure 26. Run3c without the overlaying PVA maintains the same SLP level seen as a deepening of yellow (height above control) in the same area. By the 60 hour forecast the 500 mb PVA is lost (figure not shown) and the low pressure system for the control run loses the upper level support and therefore fills. After the upper PVA diminished Run3c SLP heights continue to be greater than the control SLP as seen in Figure 27.

b. Case 4

Figure 28 shows the comparison of the thermal advection between the control run and Run3c for the active period at the 138 hour forecast. The control run had a more developed cyclonic structure at 700 mb as can be seen by the deeper low pressure contours over Italy. The 1000-500 mb thickness contours appear to have the classic self-development structure associated with cyclonic development at the surface. Stronger thermal advection can also be seen for the control run by the deeper shade of yellow in eastern Europe. A preexisting surface low pressure system took advantage of the thermal advection and deepens as can be seen by the extension of the 1000 mb contour within the

core of the cyclone as can be seen in Figures 29 and 30. Run3c maintains the pressure of the surrounding 1020 mb pressure surface for the entire period.

3.   **Central Pressure Low**

In both the active and the inactive period, there was a notable low pressure development near the center of the domain for the control run. There was little support from the Petterssen advection terms to suggest such a depression. Although the previous paragraph discussed the strengthening of the central low pressure system by thermal advection, the cyclone was already well developed by the 138 forecast when the thermal advection commenced.

For the active period, the control run low pressure system began to develop at the 102 hour forecast (figure not shown), and continues to develop into a 20 mb depression by the end of the forecast seen Figure 11. The location of the depression was in the center of the inner domain over Hungary. A similar less developed system for Run3c can be seen as a darkened blue area over western Russia.

In the inactive period, another low pressure system can be seen for the control run over Italy. Again the low pressure system was in the range of 20 mb and was located toward the center of the model domain. For this system the development began at about the 126 hour forecast.

A check was made to determine if a difference in terrain height was contributing differences in the central domain low pressure system. During the COAMPS Analysis program, a terrain height field is generated that determines the elevation parameter to use for each grid point, based on the latitude and longitude positions. As discussed earlier in section A-1, the lat/long positions do not match up perfectly between the control run and each of the test runs. The reason for this is that the grid point positioning is first determined based on the coarse grid domain, and then the domain spacing is reduced by a factor of three for the higher resolution fine grid domain. Since the comparison grid points were first based on the coarse grids, which were different (see Figure 5), the lat/long position of the fine grid points were slightly different. The differences in the lat/long positions of the control and test runs were small (see Table 1). Still, for

32

mountainous regions, the slight differences in position induced a large difference in elevation as can be seen in Figure 31. Figure 31 also shows that there is not a "problem" with the terrain height in the central area of the domain that would account for the central pressure low that develops late in the forecast period. The average difference in elevation over the entire domain was less than a meter.

The low pressure systems discussed here could not be supported by the Petterssen Development advection terms calculated in this study. Some other mechanism drove the cyclogenesis. Run3c, having the largest coarse nest boundary was assumed to be the model with the closest to actual observed data, since it would have the least adverse effects from the lateral boundary. Therefore, the low pressure system observed in the control run may not actually exist. The fact that a low pressure system was generated for the active and inactive periods in the same general location at nearly the same forecast time leads to questions as to if they occurred by coincidence, or possibly by non-realistic forcing. The observed control run central domain low pressure system was not investigated further in this study. Additional COAMPS data sets would be required to see how often a low pressure system developed in the latter stages of an extended forecast, and to make further conjecture as to potential development processes. The two periods under consideration in this study were the only two of the FNMOC data set carried out past 48 forecast hours. As stated previously, a special request was made of FNMOC post study period, to extend the forecast of the two data sets under consideration for this study.

C.   CONCLUSIONS

In this thesis, an experiment was devised to determine the significance of the separation distance between the inner and outer nests of a COAMPS model run. Four COAMPS runs were used in the experiment. The first data set, used as the control, was FNMOCs European Operational Area model. The other three data sets had the same set-up parameters and settings as the control. The only difference was the size of the outer boundary area and, therefore, the outer-to-inner nest separation distance. There were only two COAMPS forecast time periods used in this study.

The COAMPS sea level pressure fields were used as the comparison fields. The choice of sea level pressure was determined by the relevance of the sea level pressure to the forecaster and more specifically, to the naval operational planner. The forecasting of weather conditions at the surface will influence the operational planner's decision making process. Forecasted weather conditions are a vital part of operational planning.

After comparing the entire domain fields between the control and the test fields, it was determined that observed differences in the models were slight. The control run used as a basis field contains a certain degree of natural variability. When the RMS difference between the control run and the test runs was compared to the natural variability of the control run, it was found that the differences between the models were insignificant. The sea level pressure as determined by the four model runs were essentially the same when the entire model domain was compared at the grid point level.

When a direct comparison of the sea level pressure fields was made between the two model runs with the largest difference in outer domain size, isolated areas of significant differences were observed. Four individual cases were studied further to see how the cyclonic development differed due solely to the coarse domain size. It was found that the COAMPS boundary domain set up could change the resultant forecasted field in isolated areas that would change the predicted cyclogenesis.

This study only looked at two forecast periods. To get a more complete understanding of how the inner and outer domain setup affects the resultant COAMPS data fields, a more extensive study should be conducted with a larger set of data. Also, only the sea level pressure was extensively compared. The only upper level considerations made were the contributions required by the Petterssen Development Equation. Additional study could be made on comparisons of the jet or the 500 mb contour level.

Another practical area of study would be to compare the four data sets with observed data to determine which of the four performed better, and if a smaller outer boundary is "close enough" to observed weather patterns.

The other area of study mentioned in the previous section would be to fully explore the possible bias of the control model toward the development of a low pressure system toward the end of the forecast period. The occurrence of the low pressure system may be boundary condition related, since it mainly showed up in the control run.

THIS PAGE INTENTIONALLY LEFT BLANK

APPENDIX A

A.   SELECTED FIGURES PRESENTED IN THE TEXT

Active Jet
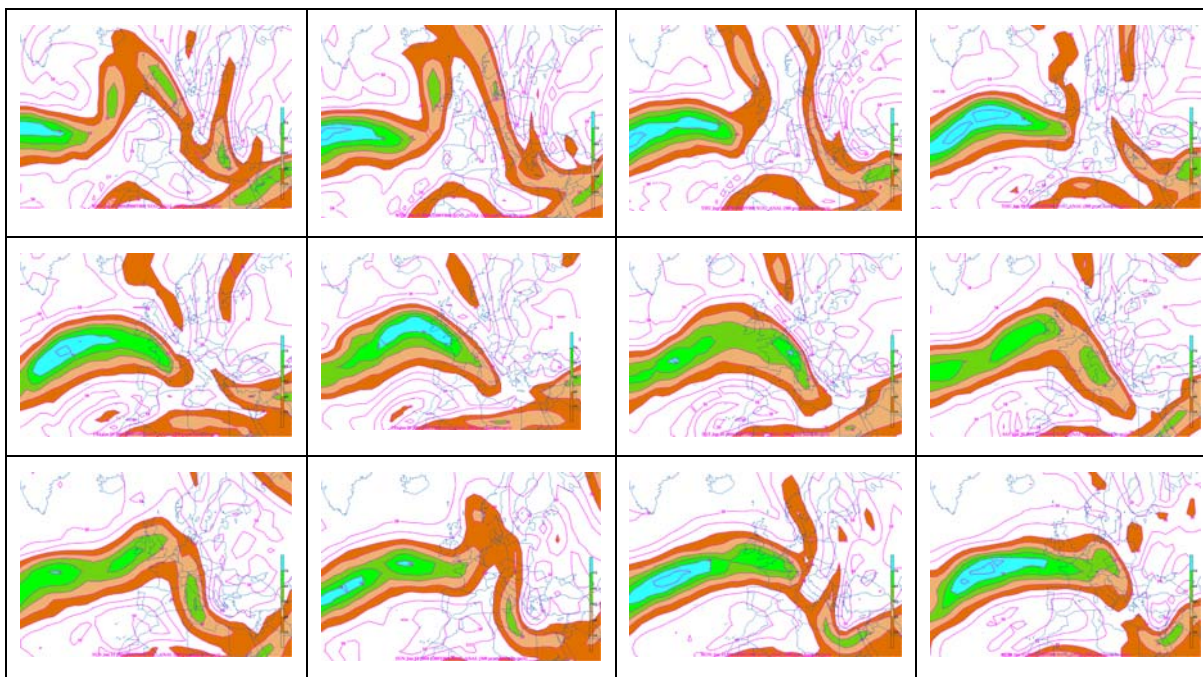
Figure 6   Jet strength determined by the 300 mb isotachs from NOGAPS Analysis model data. Units are in meters per second. Frames are given in 12 hour increments. Active jet shown on the west boundary of the COAMPS domain.
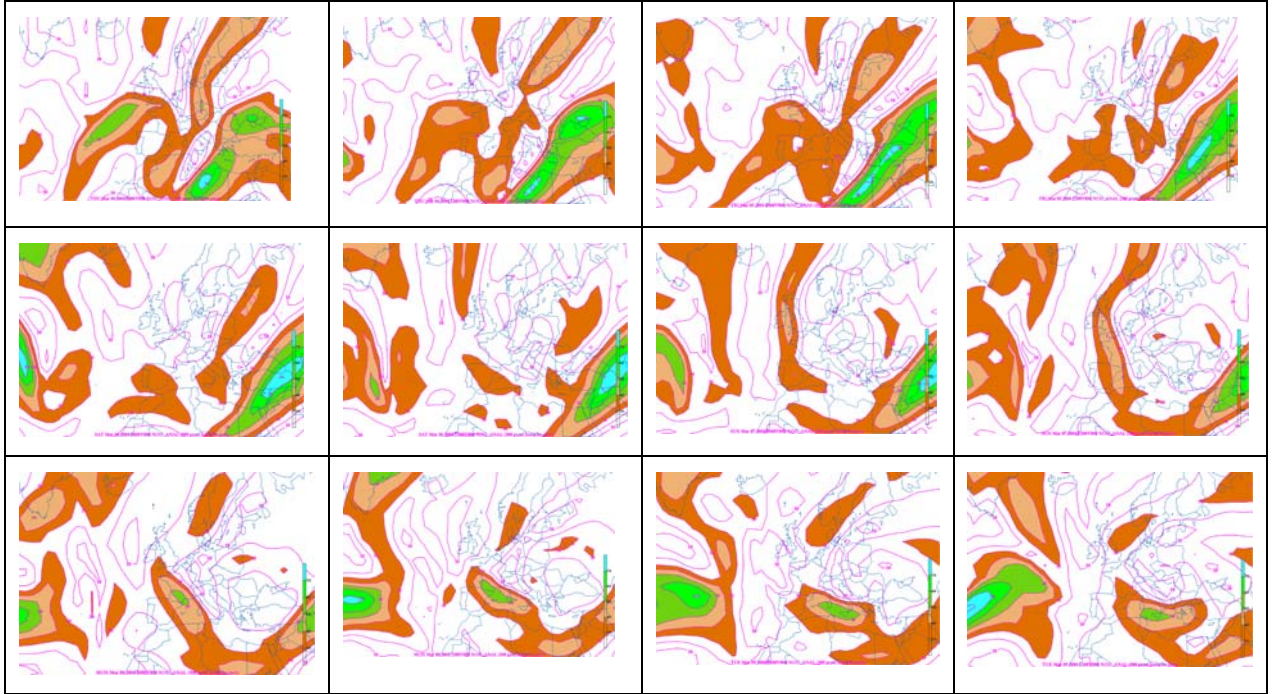
Figure 7   Jet strength determined by the 300 mb isotachs from NOGAPS Analysis model data. Units are in meters per second. Frames are given in 12 hour increments. Inactive jet period shown as a non consistent flow on the western boundary of the COAMPS domain.
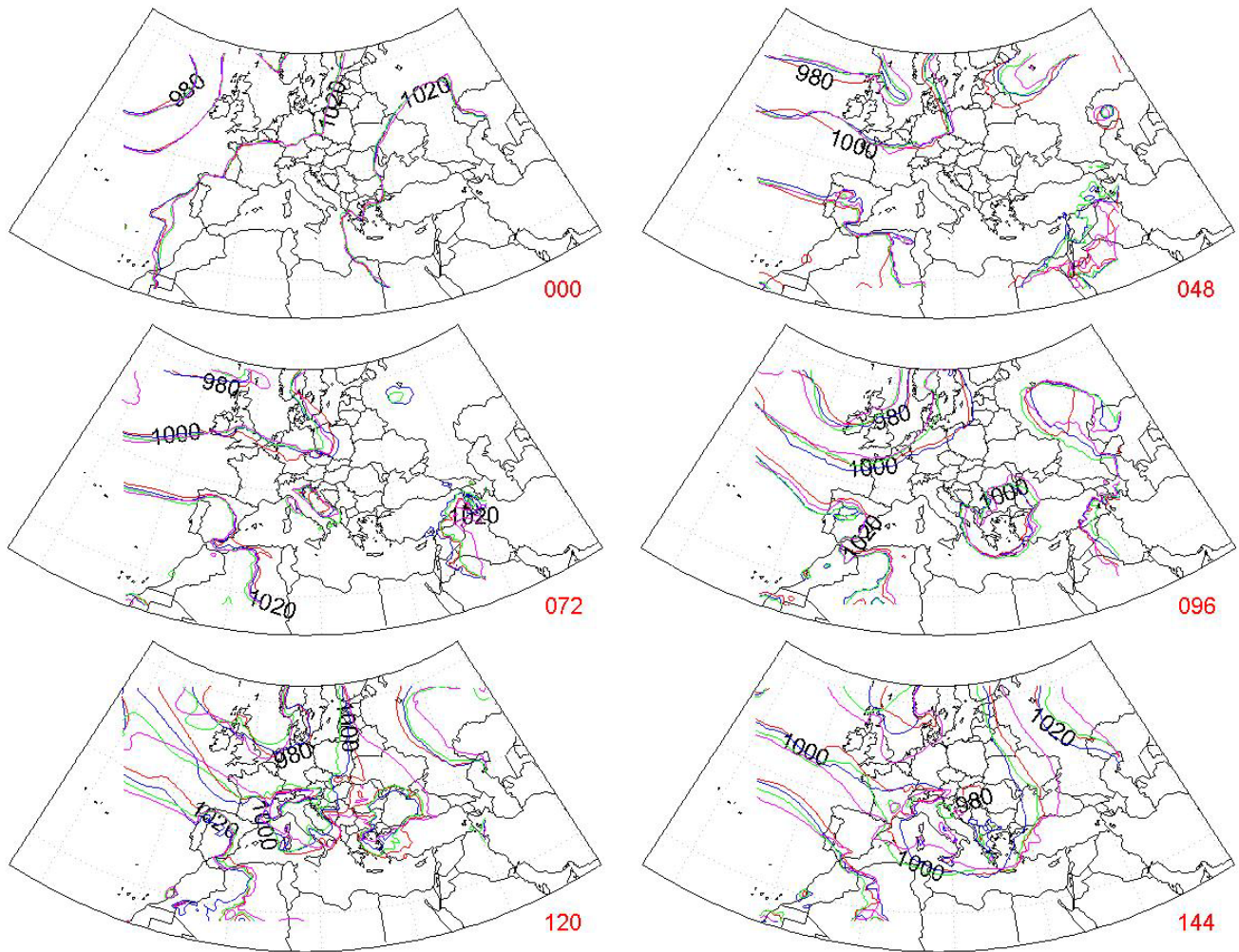
Figure 8   Sea Level Pressure contours for the active period.   Forecast hour given in the lower right hand corner. 24 hour forecast not available for analysis.
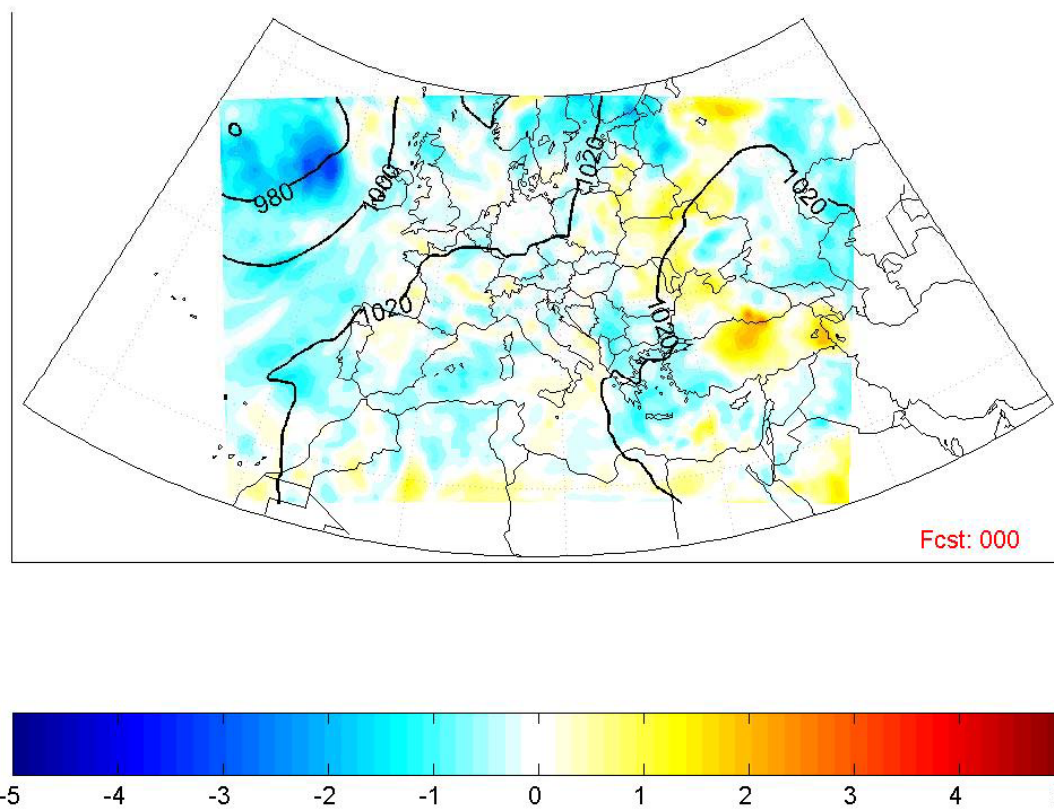
Figure 9   Horizontal depiction for the active period, '000' forecast SLP difference between Run3c and the control run. Only slight differences of less than 5 mb are present. Control run contour lines are given in black. Blue areas represent areas where Run3c contour is below the control run. Red/Yellow areas represent areas where Run3c contour is above the control run.

Figure 10 Horizontal depiction for the active period, 120 hour forecast SLP difference between Run3c and the control run. Control run contour lines are given in black. Blue areas represent areas where Run3c contour is below the control run. Red/Yellow areas represent areas where Run3c contour is above the control run.

Figure 11   Horizontal depiction for the active period, 144 hour forecast SLP difference between Run3c and the control run. Control run contour lines are given in black. Blue areas represent areas where Run3c contour is below the control run. Red/Yellow areas represent areas where Run3c contour is above the control run.
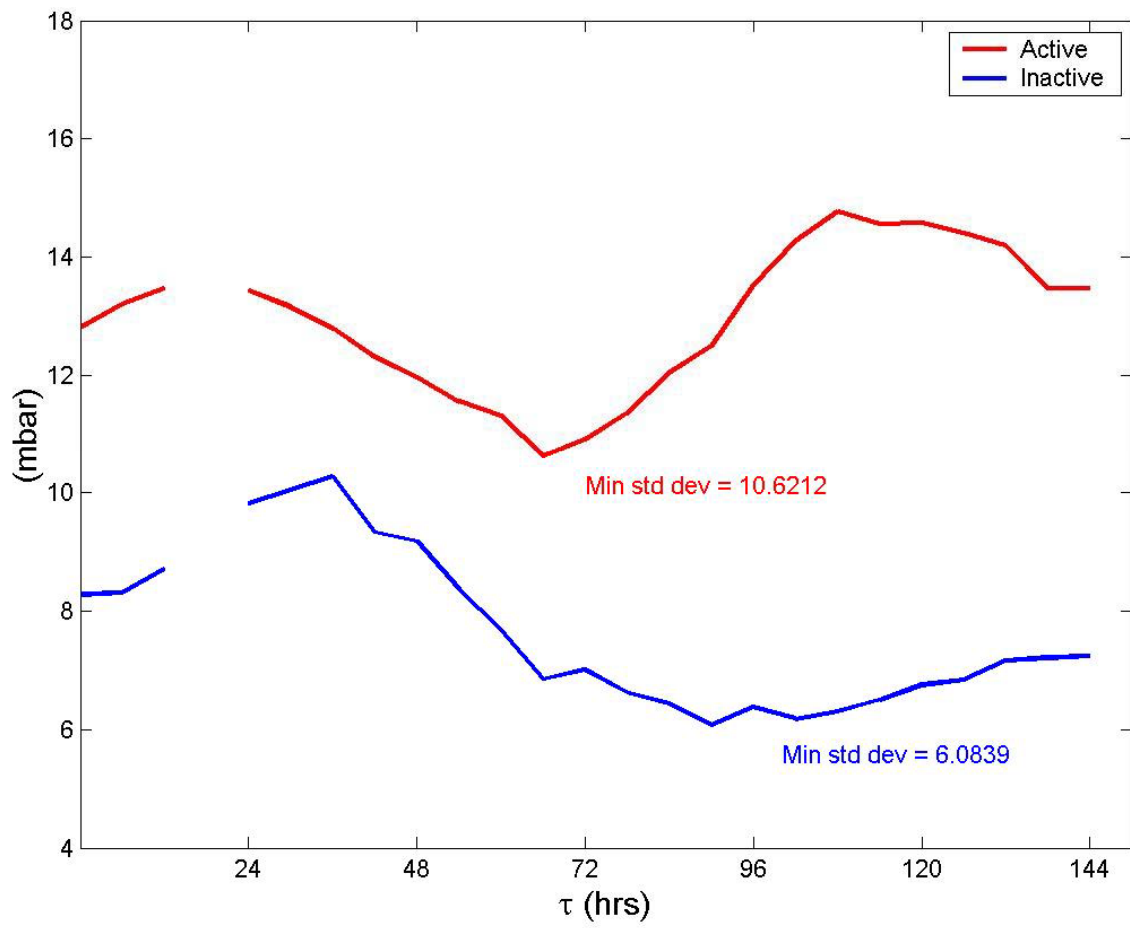
Figure 12   Standard deviation of the control run sea level pressure for both active and inactive periods.

Figure 13   Root mean square difference between the test runs and the control run, active period. The minimum standard deviation of the control run is also shown for reference. RMS of Run3a shown in blue. RMS of run3b shown in green. RMS of Run3c shown in magenta.

Figure 14   STD and RMS evaluation of domain grid points less than 990 mb, active period. Control run standard deviation is given in red. RMS difference between control run and Run3a/b/c are given in blue, green and magenta respectively.

Fcst hr	%	036	10.6	078	8.9	122	14.7
000	6.7	042	10.5	084	9.4	128	17.2
006	8.0	048	10.2	092	10.9	132	19.0
012	8.6	054	10.0	098	13.0	138	20.6
018	No data	060	9.2	104	15.3	144	25.3
024	No data	066	7.7	110	15.7		
030	10.1	072	8.2	116	14.7		

Table 2   Percentage of subset points in domain after correcting for grid mismatch.
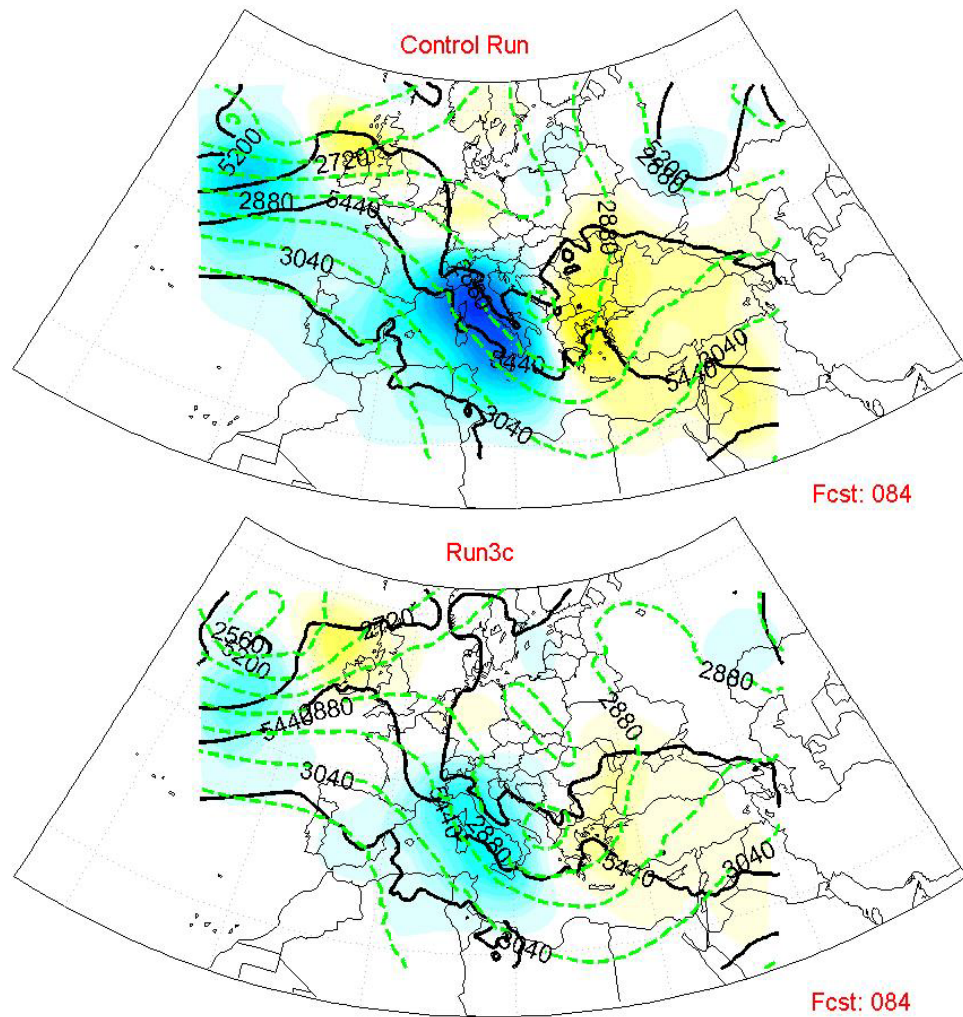
Figure 15   Comparison of the control run and Run3c Thermal Advection at the 84 hr
forecast, active period. 700 mb contour lines shown as dashed green lines.
500-1000 mb thickness line shown in black. Positive thermal advection
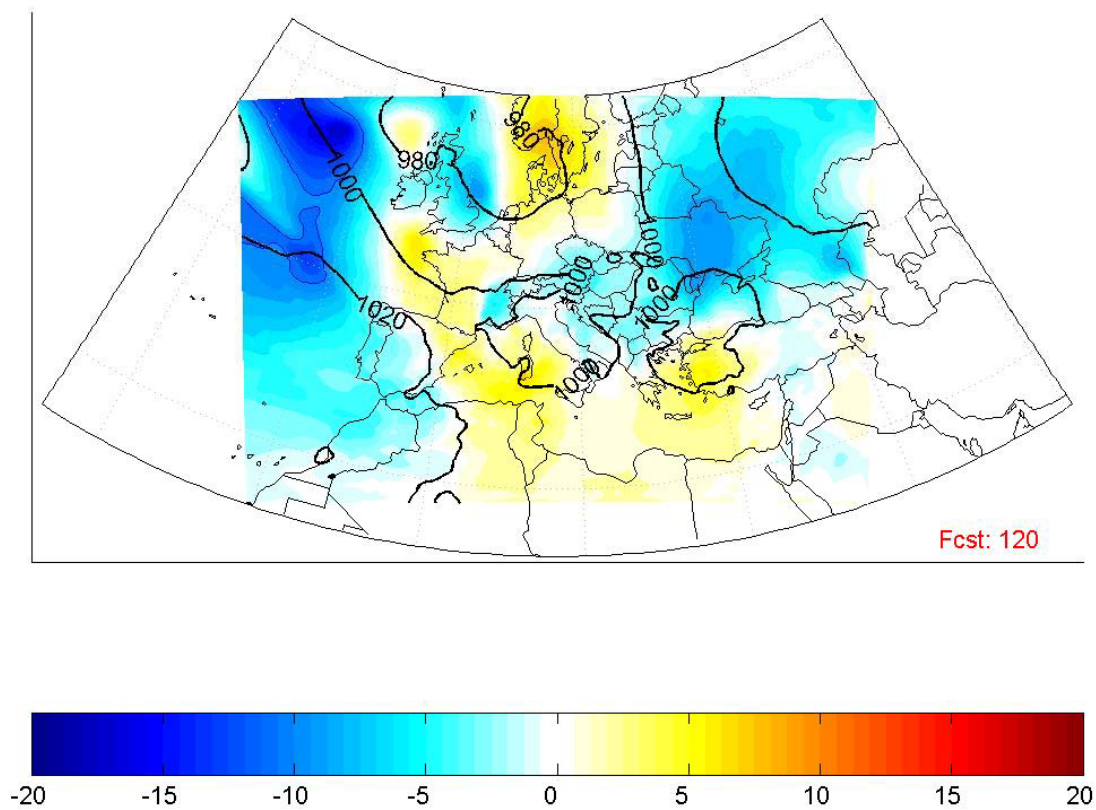shown as yellow/red areas. Negative thermal advection shown in blue.
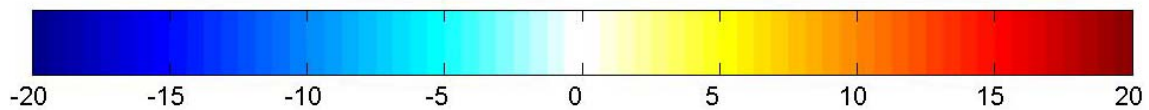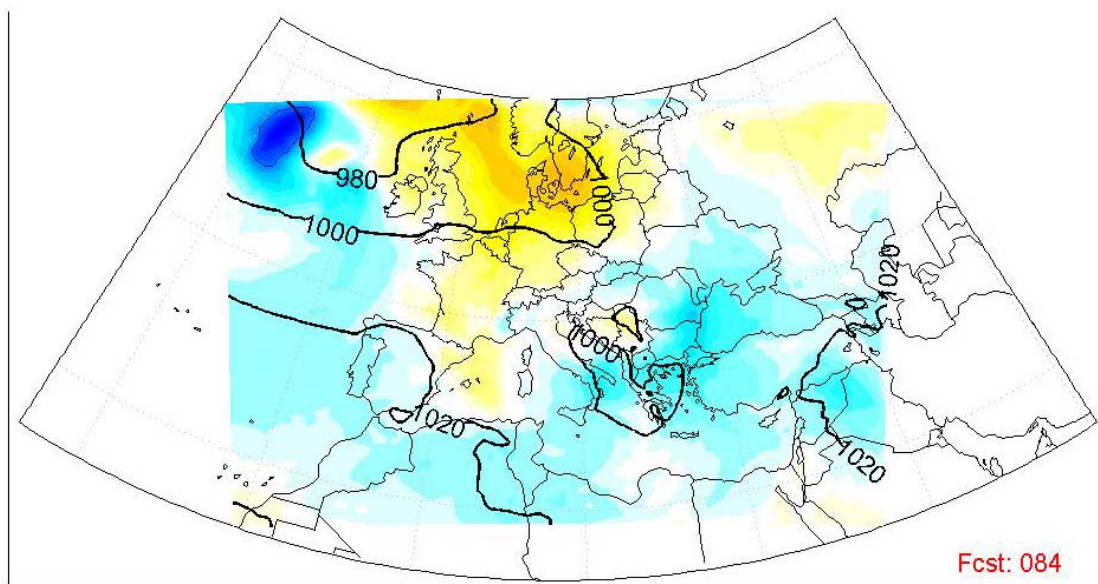
Figure 16   Horizontal depiction for the active period, 78 and 84 hour forecast SLP
difference between Run3c and the control run. Control run contour lines
are in black. Shaded areas represent same level differences as before.

47

Figure 17   Comparison of the control run and Run3c Vorticity Advection at the 96 hr forecast, active period.   500 mb contour lines shown in black.   Red contours indicate positive relative vorticity.   Blue contours indicate negative relative vorticity. The contour intervals are the same for both the positive and the negative vorticity. Positive relative vorticity advection shaded in yellow/red. Negative relative vorticity advection shaded in blue.
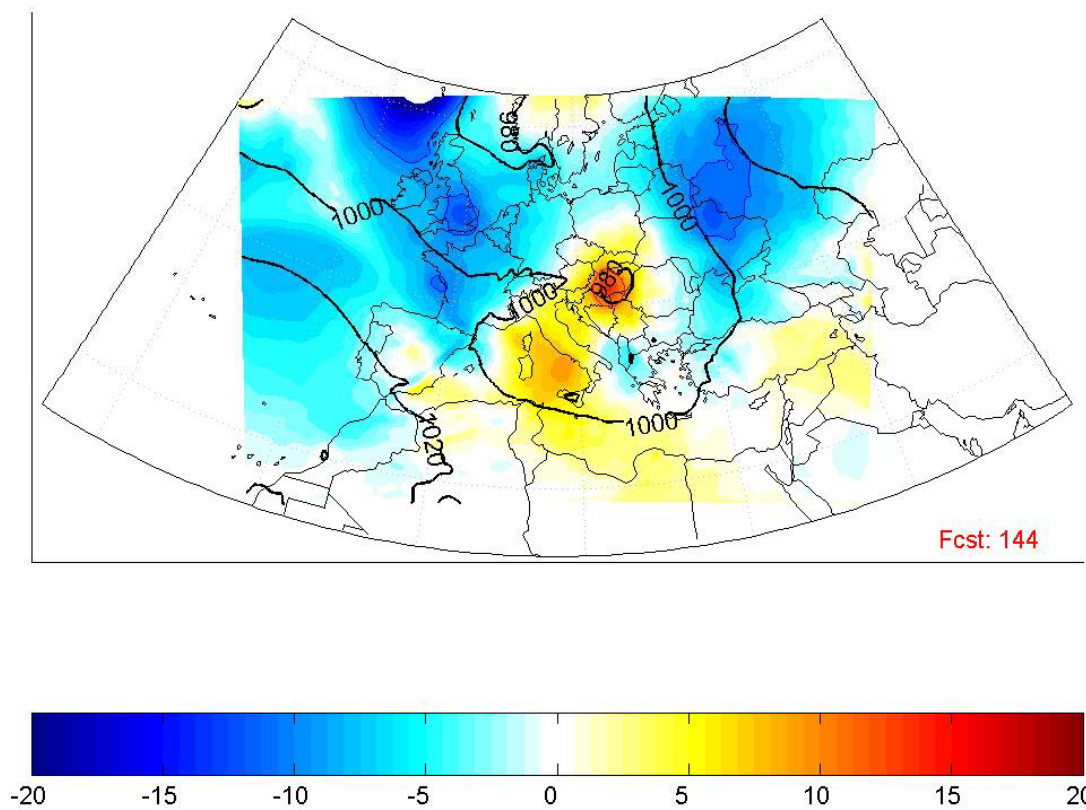
Figure 18   Horizontal depiction for the active period, 90 and 96 hour forecast SLP difference between Run3c and the control run. Control run contour lines are in black. Shaded areas represent same level differences as before.
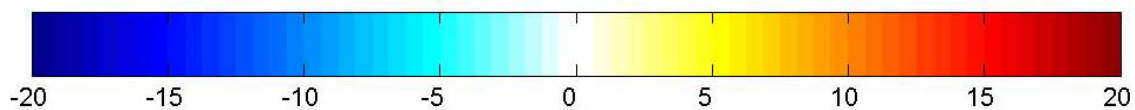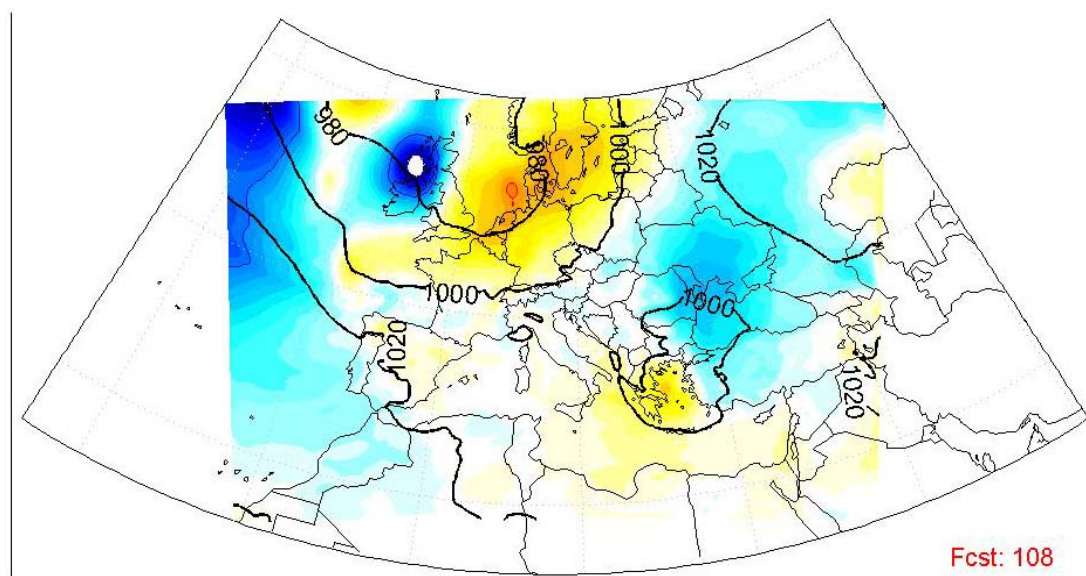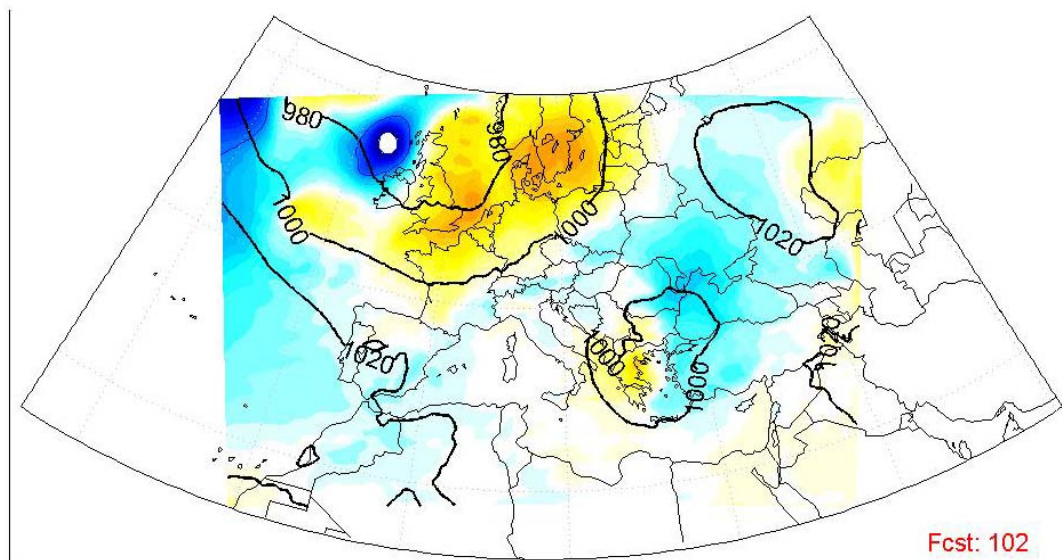
Figure 19   Horizontal depiction for the active period, 102 and 108 hour forecast SLP
difference between Run3c and the control run. Control run contour lines
are in black. Shaded areas represent same level differences as before.
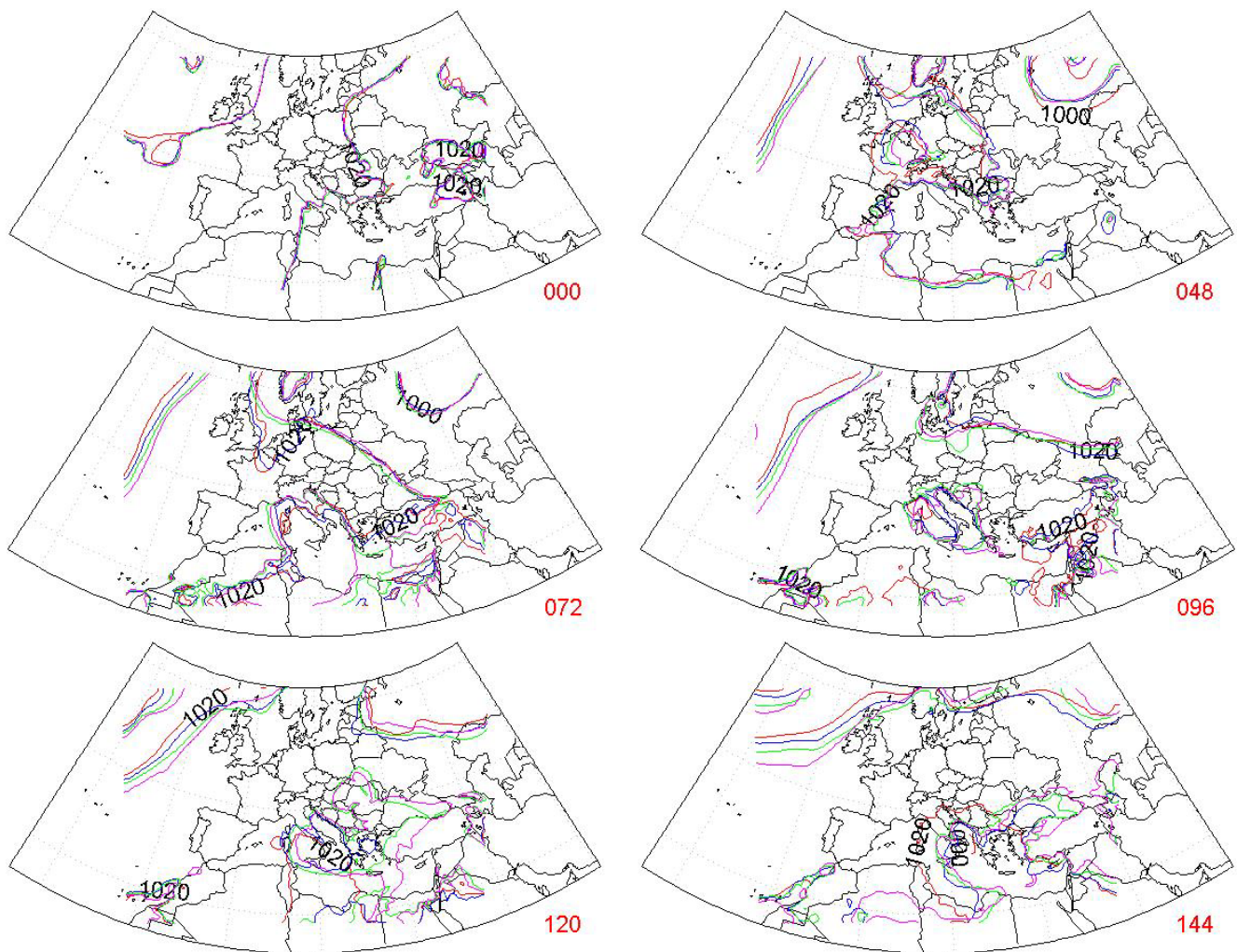
Figure 20   Sea Level Pressure contours for the inactive period. Forecast hour given in the
lower right hand corner. 24 hour forecast not available for analysis.
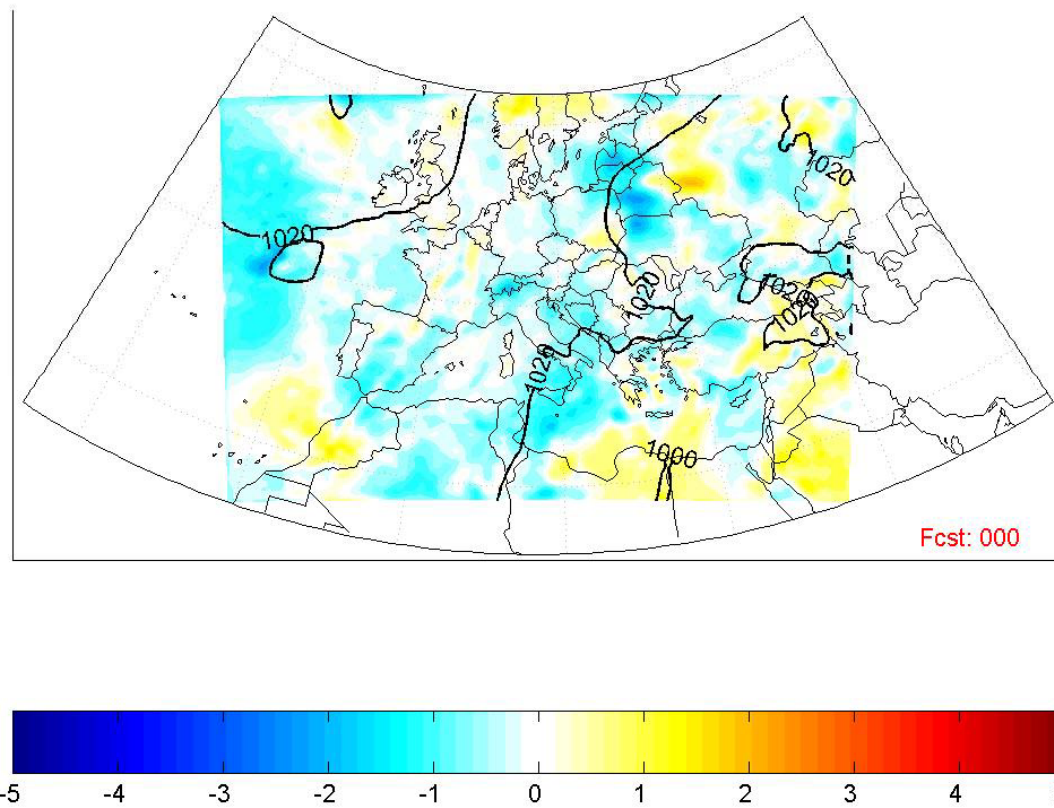
Figure 21   Horizontal depiction for the inactive period, '000' forecast SLP difference between Run3c and the control run. Only slight differences of less than 5 mb are present. Control run contour lines are given in black. Blue areas represent areas where Run3c contour is below the control run. Red/Yellow areas represent areas where Run3c contour is above the control run.
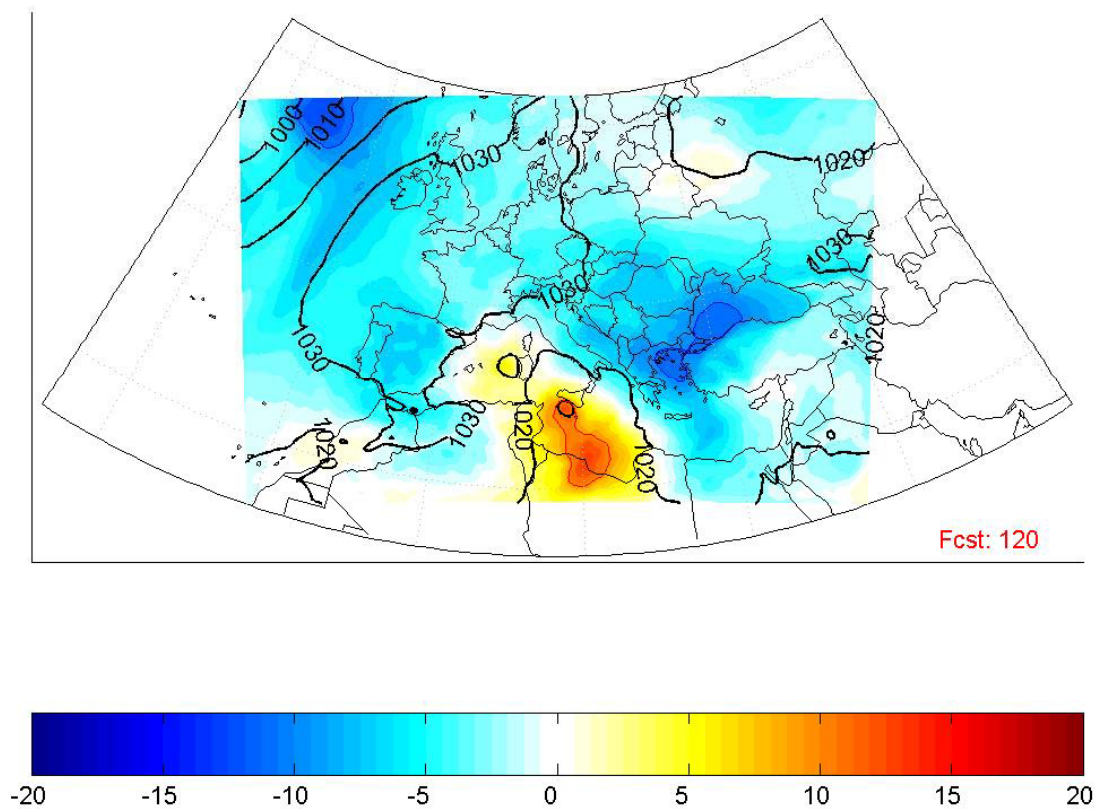
Figure 22   Horizontal depiction for the inactive period, 120 hour forecast SLP difference between Run3c and the control run. Control run contour lines are given in black. Blue areas represent areas where Run3c contour is below the control run. Red/Yellow areas represent areas where Run3c contour is above the control run.
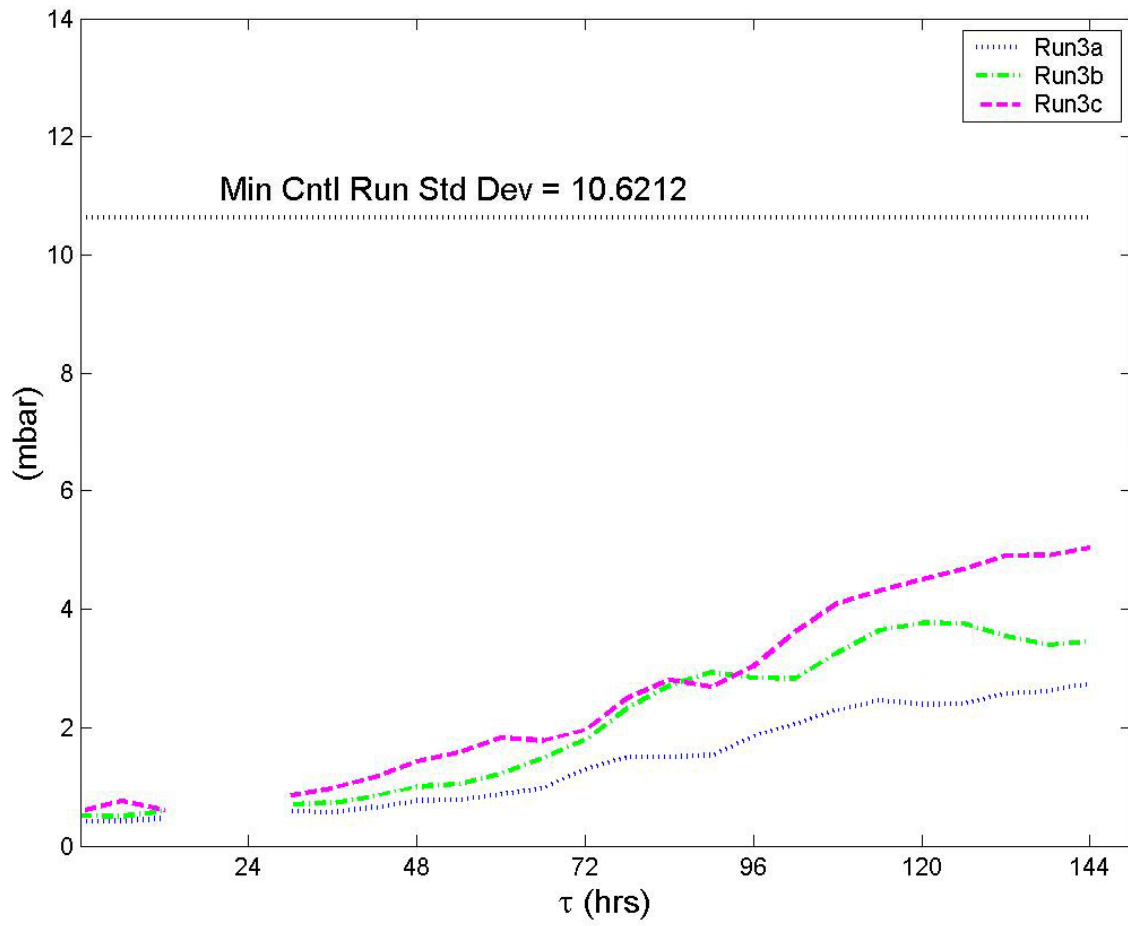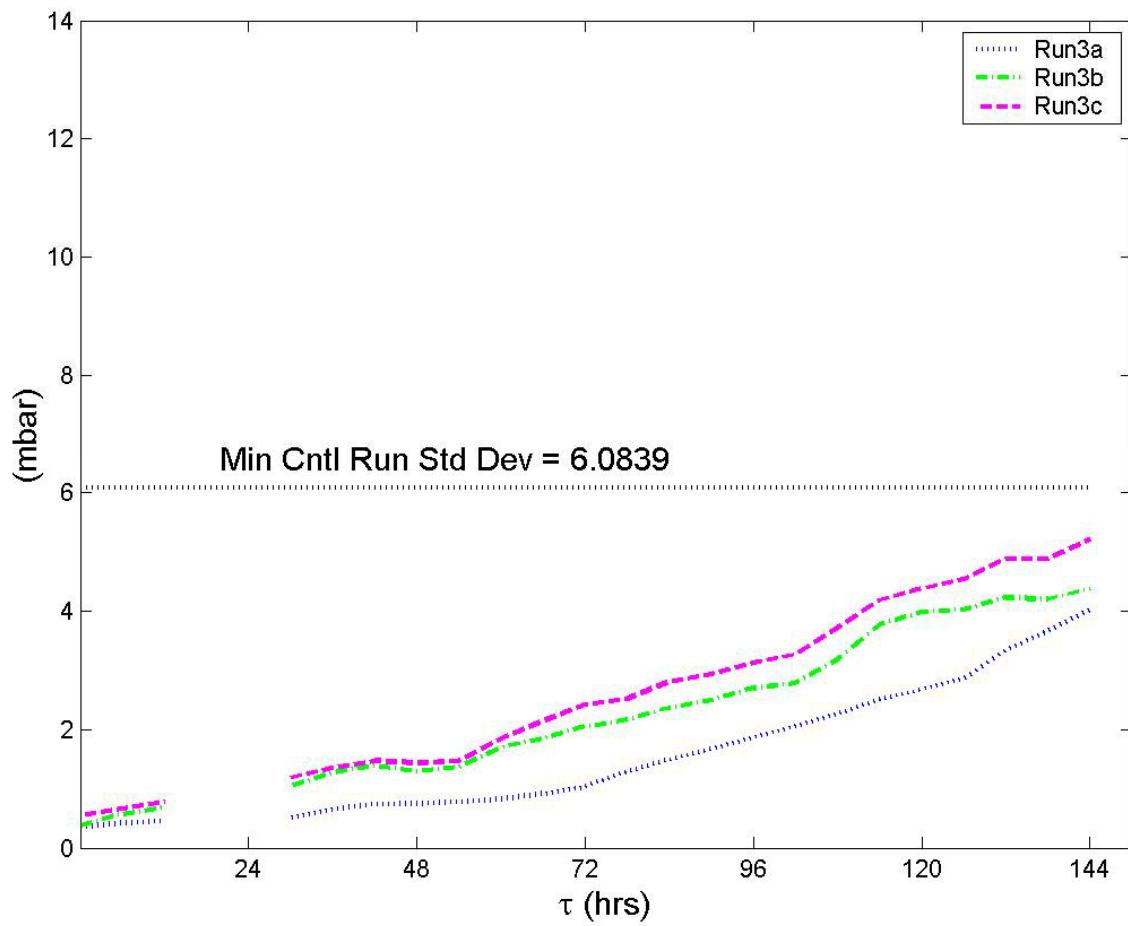
Figure 23   Root mean square difference between the test runs and the control run, inactive period. The minimum standard deviation of the control run is also shown for reference. RMS of Run3a shown in blue. RMS of run3b shown in green. RMS of Run3c shown in magenta.
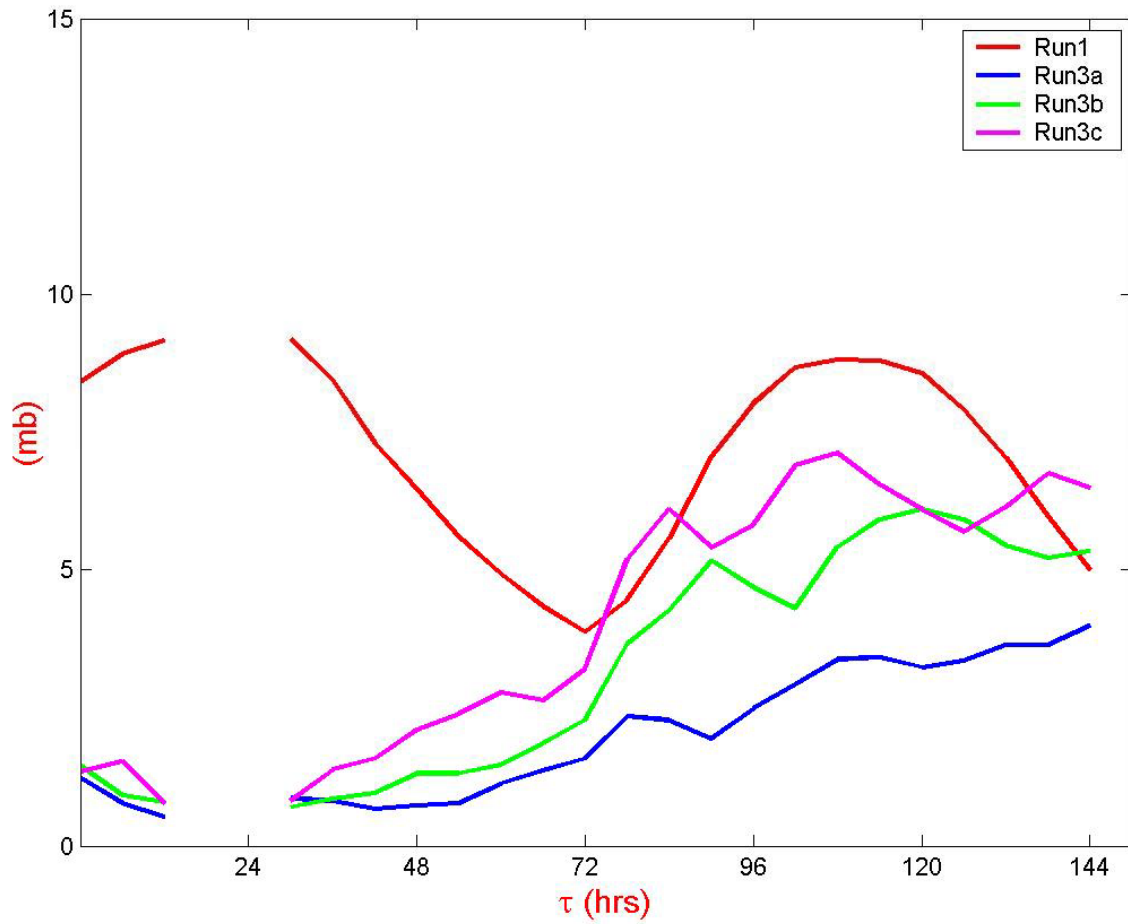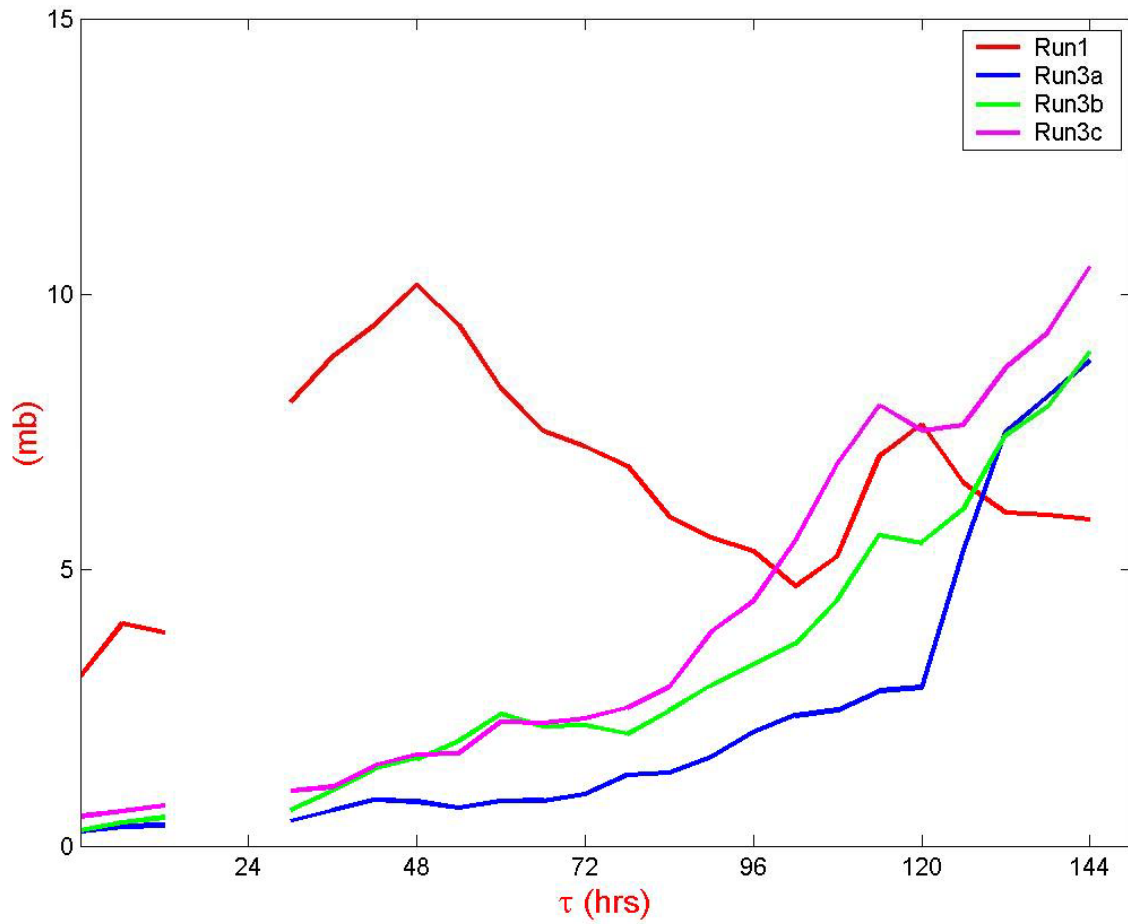
Figure 24   STD and RMS evaluation of domain grid points less than 1010 mb, inactive period.   Control run standard deviation is given in red.   RMS difference between control run and Run3a/b/c are given in blue, green and magenta respectively.

Fcst hr	%	036	23.7	078	10.8	122	4.3
000	12.6	042	17.5	084	9.2	128	5.9
006	17.3	048	15.1	092	8.0	132	6.4
012	23.9	054	15.2	098	8.5	138	6.3
018	No data	060	13.6	104	8.2	144	6.6
024	No data	066	9.9	110	6.0		
030	26.0	072	10.5	116	4.4		

Table 3   Percentage of subset points in domain after correcting for grid mismatch.
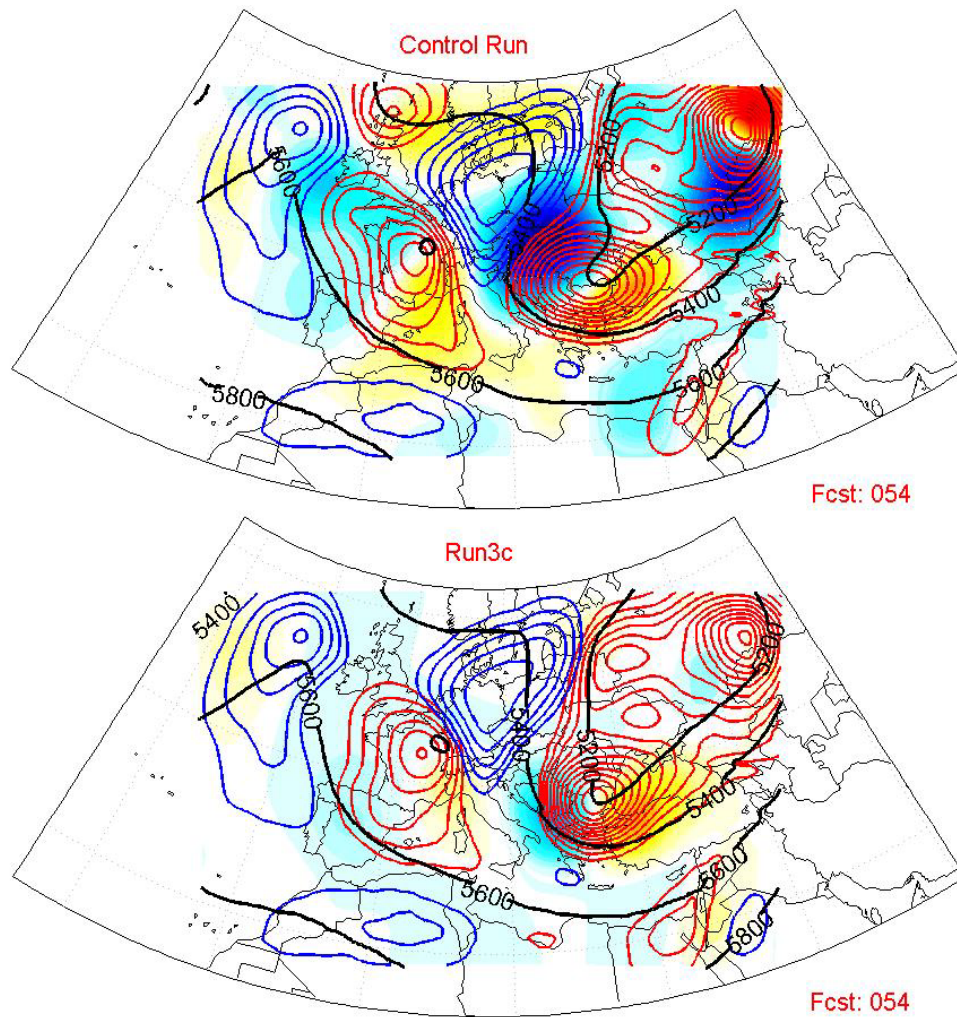
Figure 25   Comparison of the control run and Run3c Vorticity Advection at the 54 hr forecast, inactive period. 500 mb contour lines shown in black. Red contours indicate positive relative vorticity.   Blue contours indicate negative relative vorticity. Positive relative vorticity advection shown as yellow/red shaded areas. Negative relative vorticity advection shown as shaded blue areas.
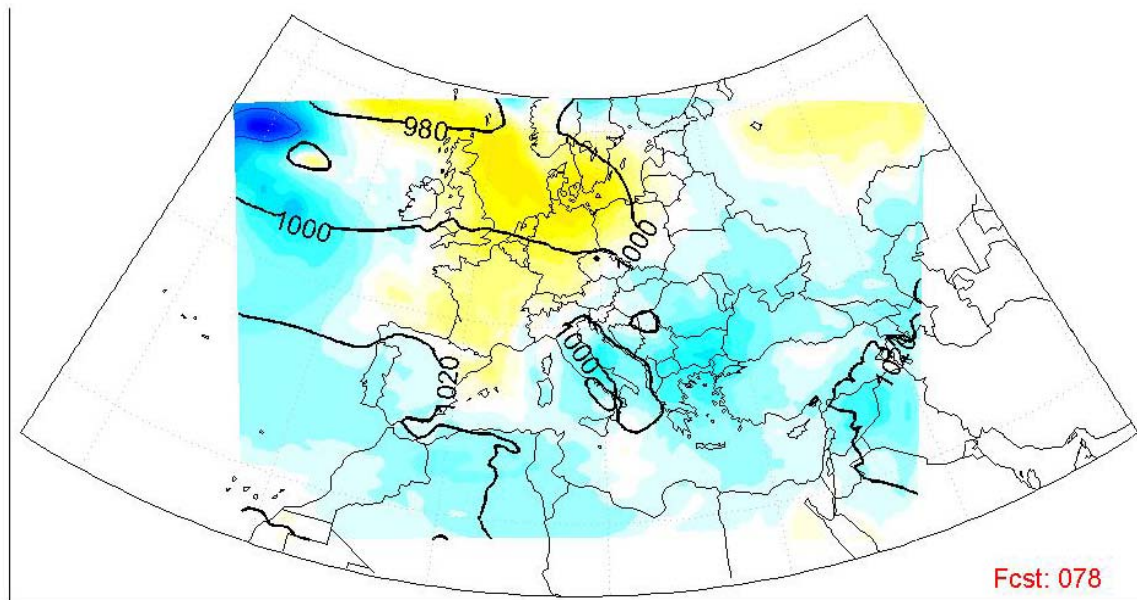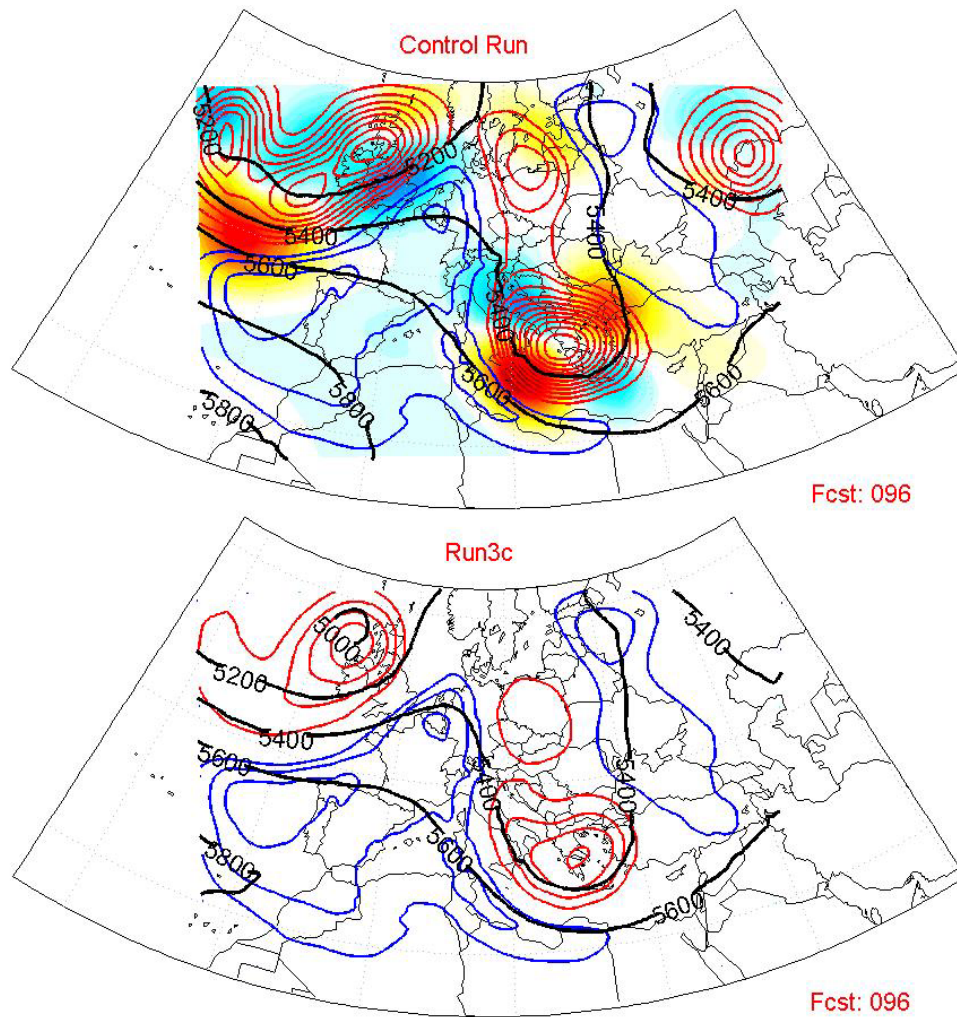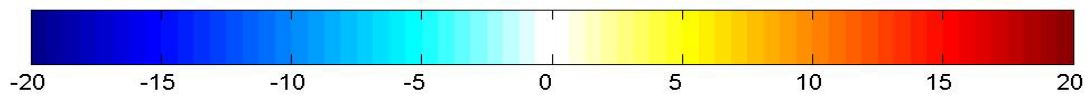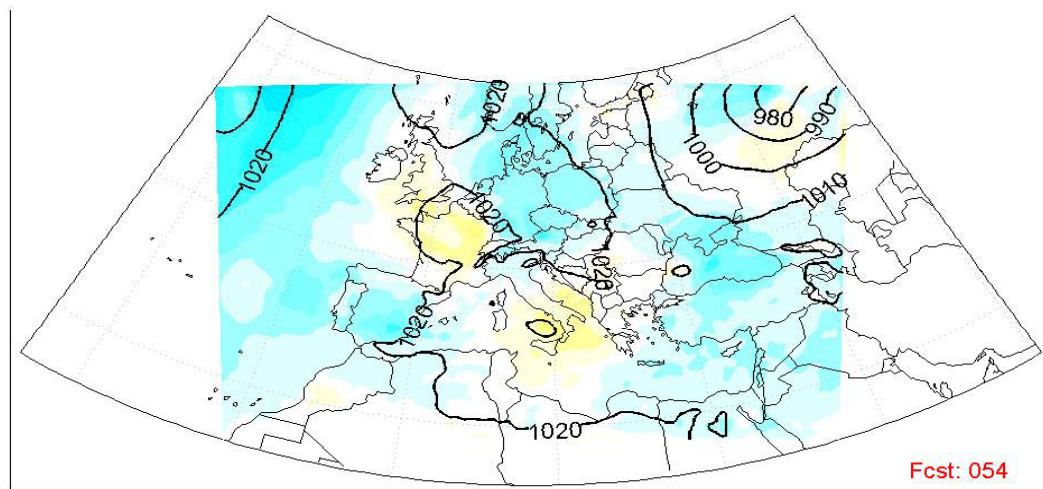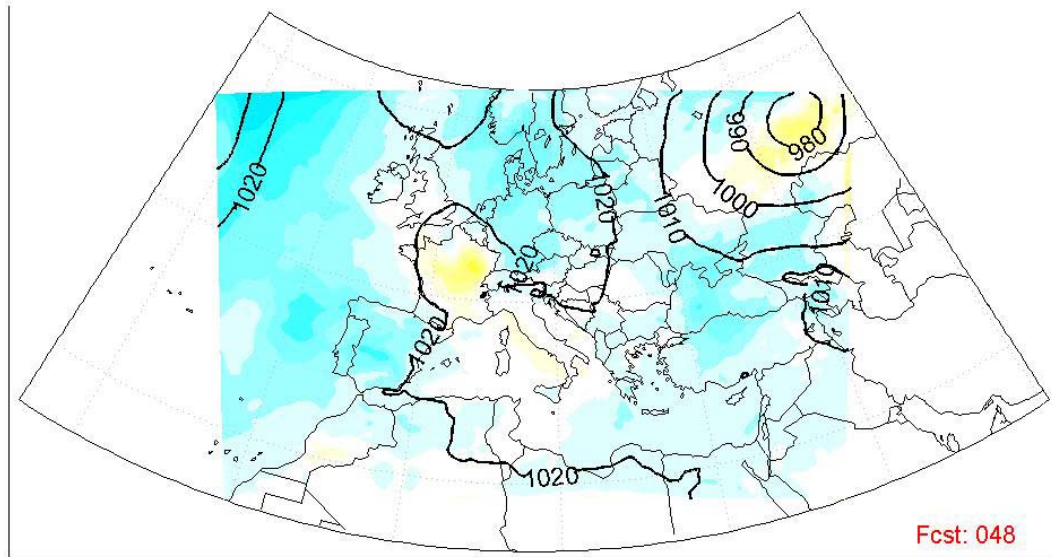
Figure 26 Horizontal depiction for the inactive period, 48 and 54 hour forecast SLP difference between Run3c and the control run. Control run contour lines are in black. Shading represents the same level differences as before.
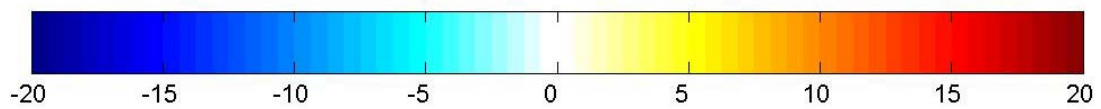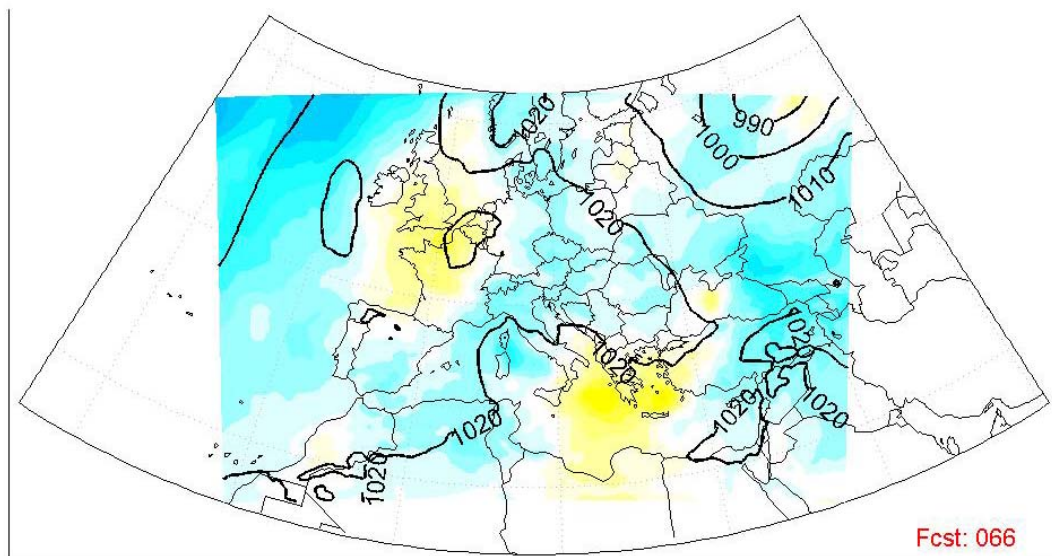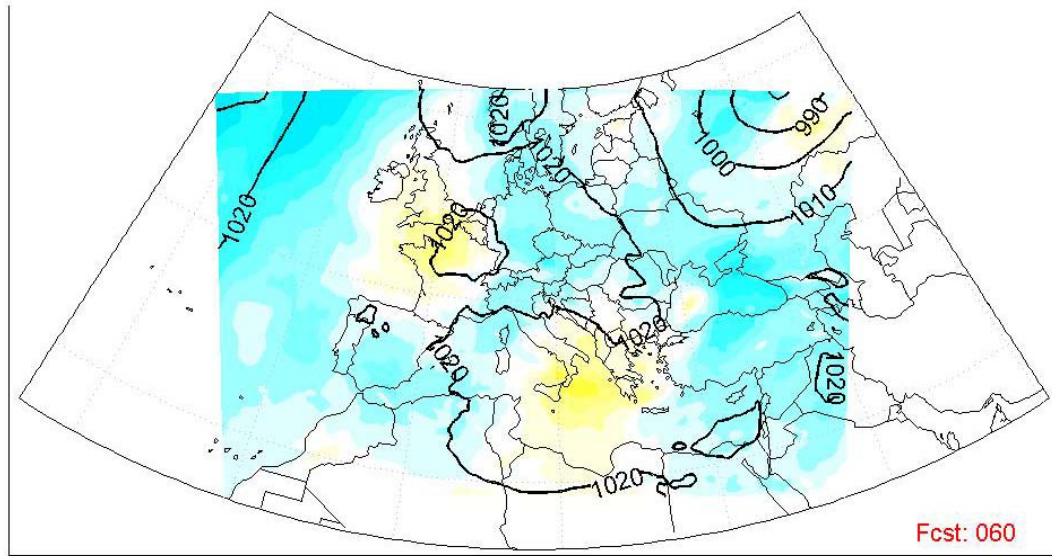
Figure 27   Horizontal depiction for the inactive period, 60 and 66 hour forecast SLP
           difference between Run3c and the control run. Control run contour lines
           are in black. Shading represents the same level differences as before.
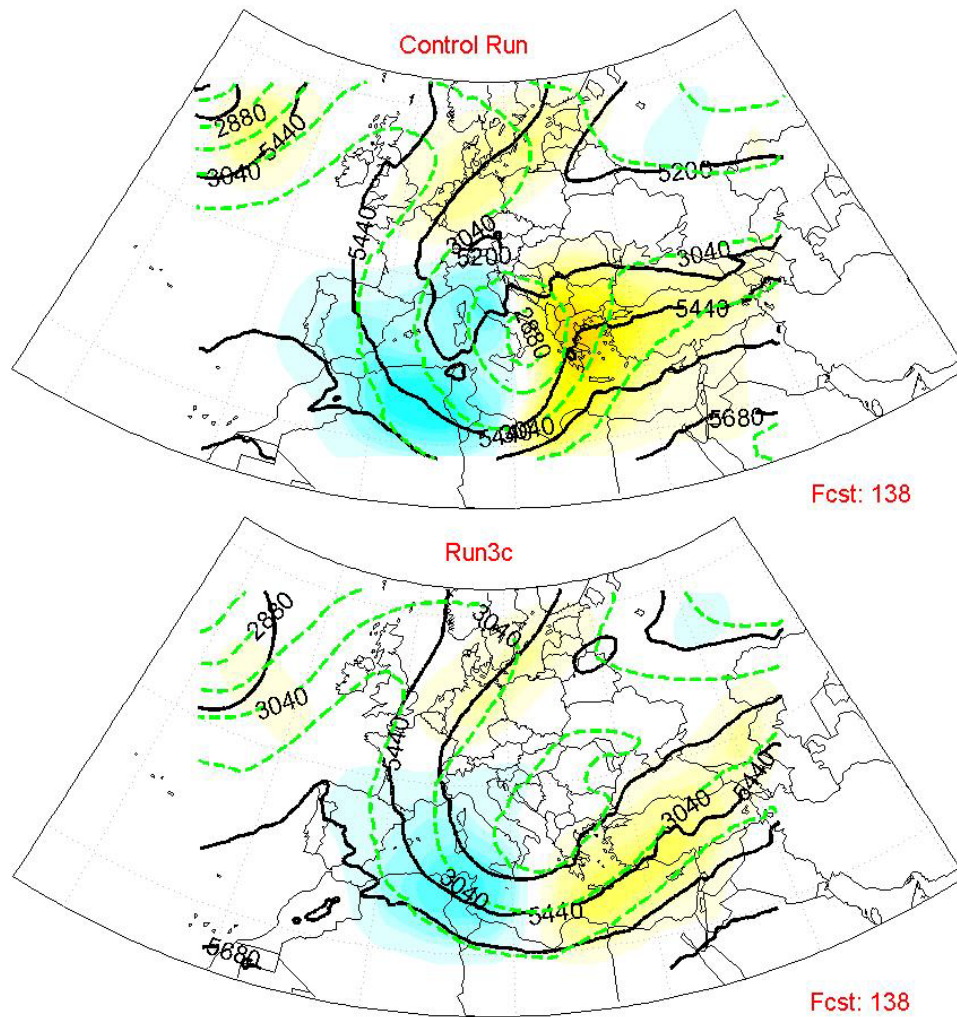
Figure 28   Comparison of the control run and Run3c Thermal Advection at the 138 hr forecast, inactive period. 700 mb contour lines shown as dashed green lines.   500-1000 mb thickness line shown in black.   Positive thermal advection shown as yellow/red areas. Negative thermal advection shown in blue.
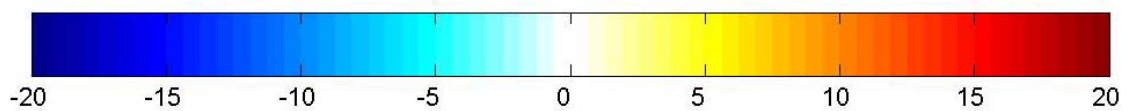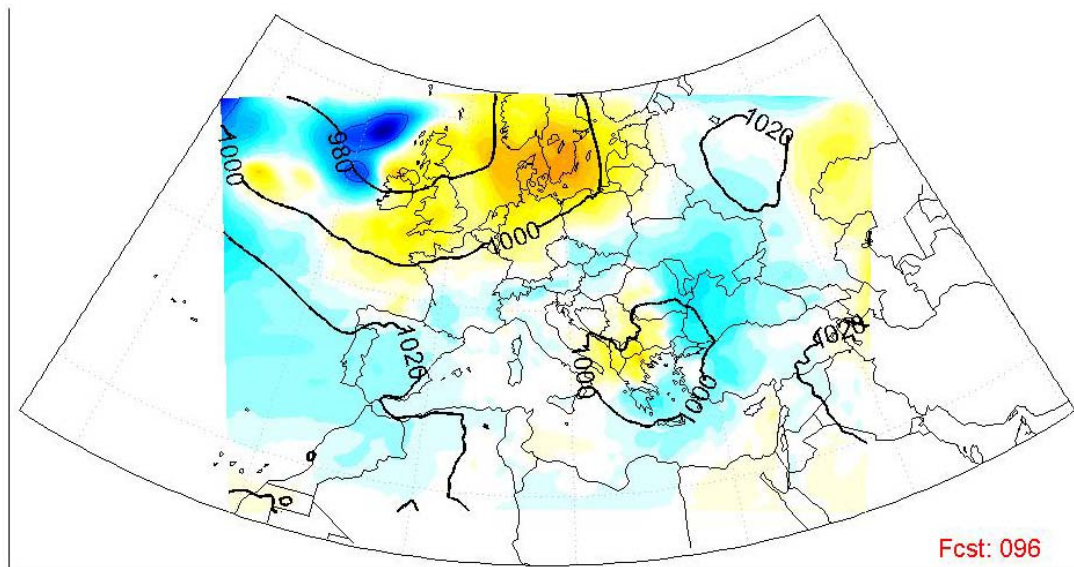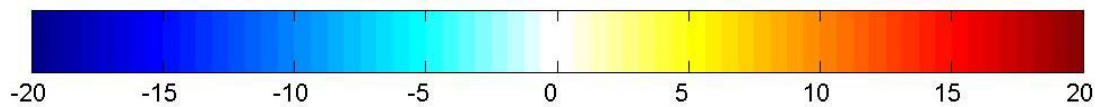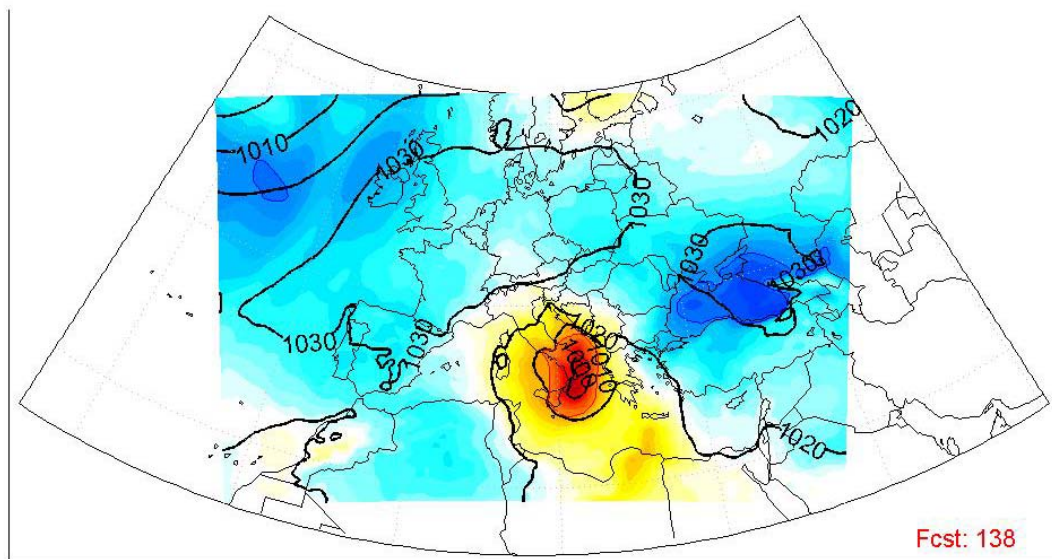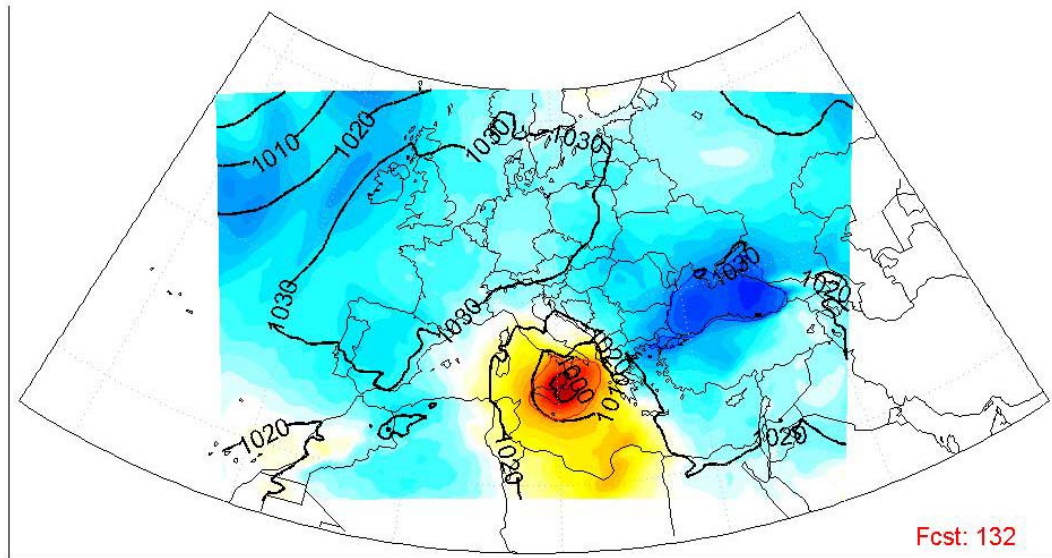
Figure 29   Horizontal depiction for the inactive period, 132 and 138 hour forecast
SLP difference between Run3c and the control run. Control run contour
lines are in black. Shading represents the same level differences as before.
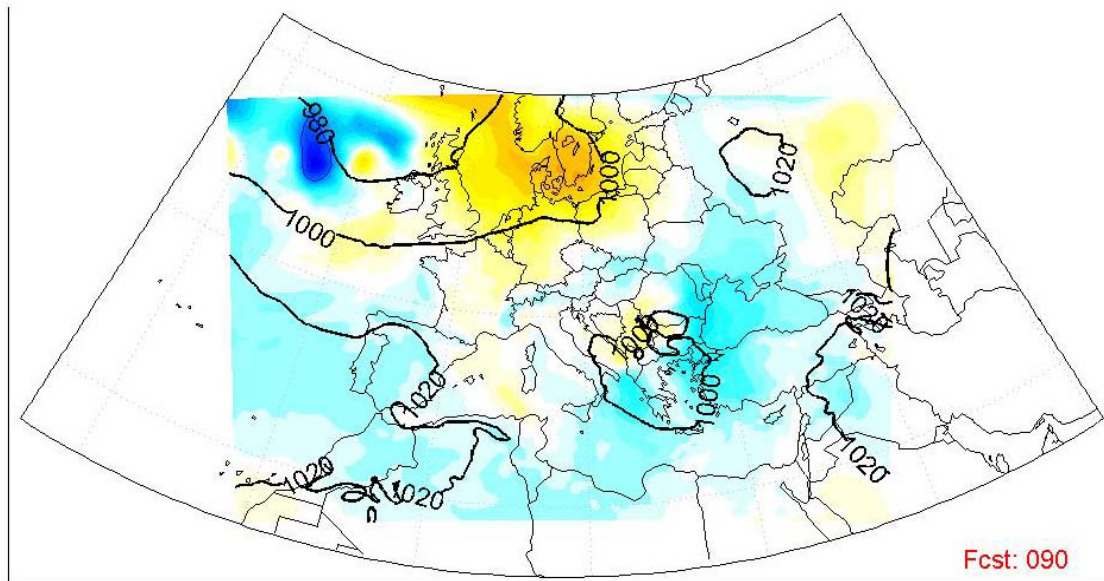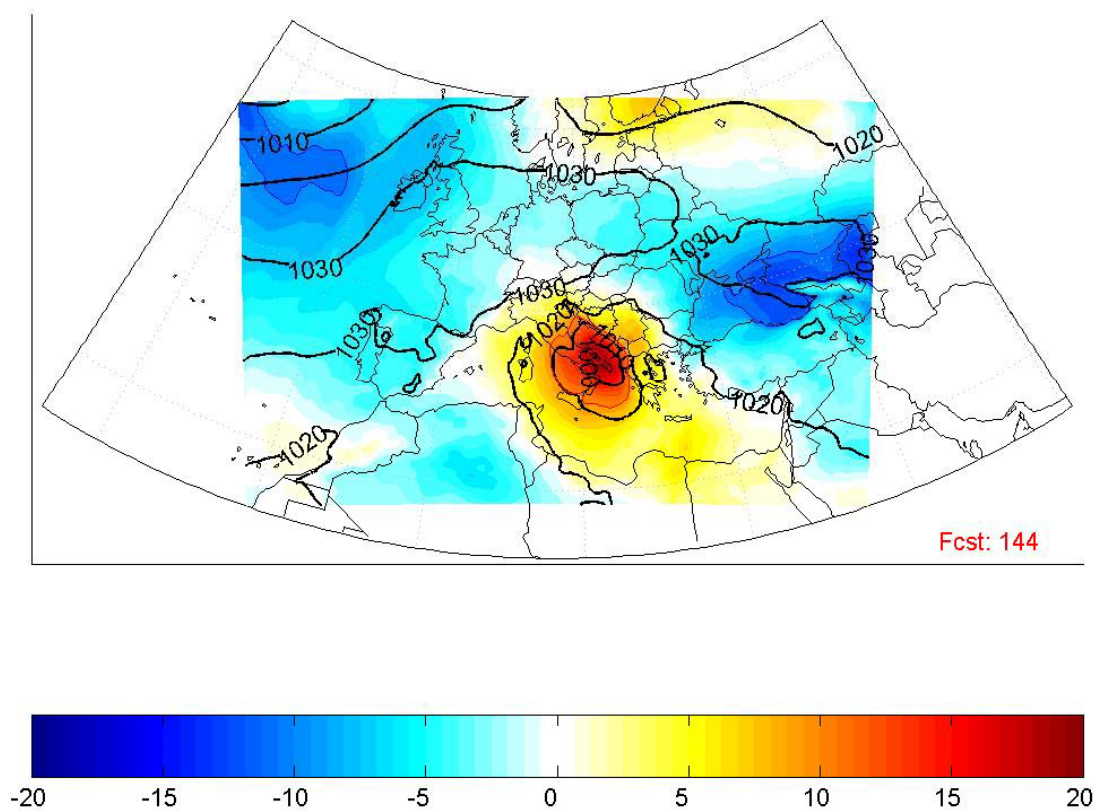
Figure 30   Horizontal depiction for the inactive period, 144 hour forecast SLP difference between Run3c and the control run. Control run contour lines are in black. Shading represents the same level differences as before.
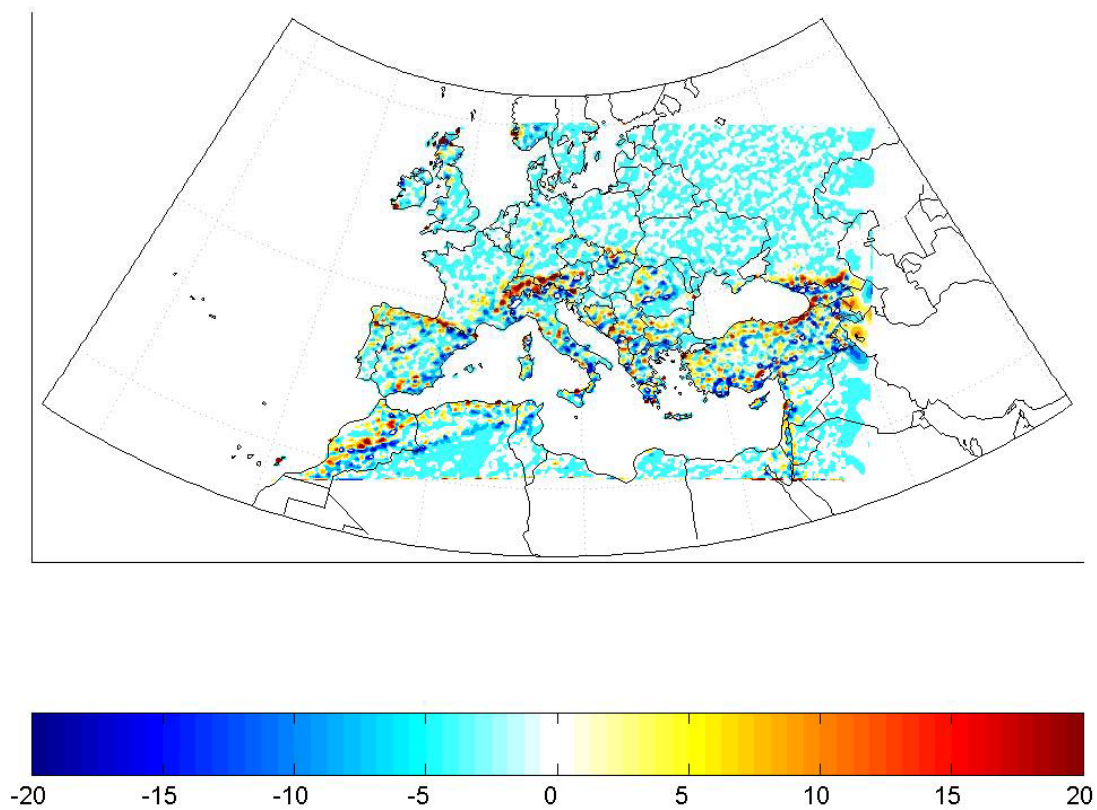
Figure 31   Terrain height difference between control run and Run3c in meters. Although the scale is only given for up to 20 meters difference, actual differences in isolated areas were as high as 470 meter. The mean height difference was 0.38 meters with a standard deviation of 12.8 meters.

APPENDIX B

A. EQUATIONS USED IN NOGAPS MODEL (FROM HOGAN AND ROSMOND, 1991)

The equations for the NOGAPS model are formulated in a spherical coordinates and a hybrid vertical coordinate. The horizontal coordinates are the longitude λ and the latitude φ. The vertical coordinate is represented by η and has a range from 0 to 1.0. From the principle of mass continuity

$$\frac{\partial \pi}{\partial t} = -\int_0^1 \nabla\bullet\left(\mathbf{u}\,\frac{\partial p}{\partial \eta}\right) d\eta - \int_{p_{top}}^{p_s} \nabla\bullet\left(\mathbf{u}\,dp\right), \tag{0.24}$$

where π is defined as

$$\pi = p_s - p_{top} \tag{0.25}$$

$p_{top} = 1\text{mb}$ is the pressure at the top of the model; p_s is the terrain pressure; and dp is a function of λ, φ, and η. The vertical motion equation is

$$\left[\dot{\eta}\frac{\partial p}{\partial \eta}\right](\eta) = B(\eta)\frac{\partial \pi}{\partial t} - \int_0^{\eta} \nabla\bullet\left(\mathbf{u}\,\frac{\partial p}{\partial \eta}\right) d\eta, \tag{0.26}$$

where

$$B(\eta) = \frac{p(\lambda,\varphi,\eta) - p_{top}}{\pi(\lambda,\varphi)}. \tag{0.27}$$

The thermodynamic variable used by the forecast model is the virtual potential temperature θ, which is defined by

$$\theta = T\left(\frac{1 + 0.608q}{P}\right) \tag{0.28}$$

where q is the specific humidity. The function P is defined as

$$P = \left(\frac{p}{p_0} \right)^{\kappa} \tag{0.29}$$

where p_0 is 1000 hPa and κ is the gas constant divided by the heat capacity, $\kappa = R/c_p$. The thermodynamic equation is given by

$$\frac{\partial \theta}{\partial t} = \left(\frac{\partial \theta}{\partial t} \right)_{adv} + Q_\theta, \tag{0.30}$$

where Q_θ is the diabatic heating. The quantity Q_θ is the sum of the radiation, latent heat release, and the horizontal and vertical diffusion processes. The advection term is defined by

$$\left(\frac{\partial \theta}{\partial t} \right) = -\frac{u}{a \cos\varphi} \frac{\partial \theta}{\partial \lambda} - \frac{v}{a} \frac{\partial \theta}{\partial \varphi} - \dot{\eta} \frac{\partial \theta}{\partial \eta}. \tag{0.31}$$

The hydrostatic equation is written in the form

$$\frac{\partial \phi}{\partial P} = -c_p \theta \tag{0.32}$$

where ϕ is the geopotential and P is given by (0.29). The above form is chosen to facilitate total energy conservation in the discrete adiabatic equation.

For the NOGAPS spectral model, the choice of variables used to describe the atmospheric motion is the vorticity ζ and the divergence D. The ζ and the D equations are given by

$$\frac{\partial \zeta}{\partial t} = -\frac{1}{\cos^2\varphi} \frac{\partial G}{\partial \lambda} - \frac{\partial H}{\partial \mu}, \tag{0.33}$$

$$\frac{\partial D}{\partial t} = -\frac{1}{\cos^2\varphi} \frac{\partial H}{\partial \lambda} - \frac{\partial G}{\partial \mu} - \nabla^2 (\phi + I), \tag{0.34}$$

where μ, U, V, G, H, and I are defined as

$$\mu = \sin\varphi, \tag{0.35}$$

64

$$U = u \frac{\cos\varphi}{a}, \tag{0.36}$$

$$V = v \frac{\cos\varphi}{a}, \tag{0.37}$$

$$G = U\left(\zeta + 2\Omega\mu\right) + \left[\dot{\eta}\frac{\partial p}{\partial \eta}\right]\left(\frac{\partial V}{\partial p}\right)$$
$$+ \frac{c_p}{a^2}\theta\left(\frac{\partial P}{\partial \pi}\right)\left(\frac{\partial \pi}{\partial \mu}\right)\cos^2\varphi - Q_v \frac{\cos\varphi}{a}, \tag{0.38}$$

$$H = V\left(\zeta + 2\Omega\mu\right) + \left[\dot{\eta}\frac{\partial p}{\partial \eta}\right]\left(\frac{\partial U}{\partial p}\right)$$
$$- \frac{c_p}{a^2}\theta\left(\frac{\partial P}{\partial \pi}\right)\left(\frac{\partial \pi}{\partial \mu}\right)Q_u \frac{\cos^2\varphi}{a}, \tag{0.39}$$

and

$$I = \left(\frac{U^2 + V^2}{2}\right)\frac{a^2}{\cos^2\varphi}, \tag{0.40}$$

where Q_u and Q_v are the components of the momentum stress and Ω is the earth's angular rotation rate.

All the terms in the equations of motion are written in spherical harmonic form using the transform

$$X_n^m(t) = \frac{1}{2\pi}\int_{-1}^{1}\int_{0}^{2\pi} X\left(\lambda,\mu,t\right) \times P_n^m\left(\mu\right)\exp\left(-im\lambda\right)d\lambda d\mu, \tag{0.41}$$

where m is the zonal wavenumber and n the total wavenumber.

For a complete description of the NOGAPS numerical model see Hogan and Rosemond, 1991.

THIS PAGE INTENTIONALLY LEFT BLANK

APPENDIX C

A. EQUATIONS USED IN COAMPS MODEL (FROM HODUR, 1997)

The COAMPS atmospheric model is comprised of the nonhydrostatic, compressible form of the dynamics and parameterization for subgrid-scale mixing, surface fluxes, explicit moist physics, cumulus convection process and radiation. The vertical coordinate σ is chosen to allow for flow over irregular surfaces. The sigma coordinates are defined as

$$\sigma = z_{\text{top}} \left(\frac{z - z_{\text{sfc}}}{z_{\text{top}} - z_{\text{sfc}}} \right) \tag{0.42}$$

where z_{top} is the depth of the model domain and z_{sfc} is the terrain height. The complete set of prognostic equations is as follows:

$$\frac{\partial u}{\partial t} + C_p \theta_v \left(\frac{\partial \pi'}{\partial x} + G_x \frac{\partial \pi'}{\partial \sigma} \right) + K_D \left(\frac{\partial D_3}{\partial x} + G_x \frac{\partial D_3}{\partial \sigma} \right)$$
$$= -u \frac{\partial u}{\partial x} - v \frac{\partial u}{\partial y} - \sigma \frac{\partial u}{\partial \sigma} + fv + D_u + K_H \nabla^4 u \tag{0.43}$$

$$\frac{\partial v}{\partial t} + C_p \theta_v \left(\frac{\partial \pi'}{\partial y} + G_y \frac{\partial \pi'}{\partial \sigma} \right) + K_D \left(\frac{\partial D_3}{\partial y} + G_y \frac{\partial D_3}{\partial \sigma} \right)$$
$$= -u \frac{\partial v}{\partial x} - v \frac{\partial v}{\partial y} - \sigma \frac{\partial v}{\partial \sigma} - fu + D_v + K_H \nabla^4 v \tag{0.44}$$

$$\frac{\partial w}{\partial t} + C_p \theta_v G_z \frac{\partial \pi'}{\partial \sigma} + K_D G_z \frac{\partial D_3}{\partial \sigma}$$
$$= g \left(\frac{\theta'}{\theta} + 0.608 q_v' - q_v - q_r - q_i - q_s \right) \tag{0.45}$$
$$- u \frac{\partial w}{\partial x} - v \frac{\partial w}{\partial y} - \dot{\sigma} \frac{\partial w}{\partial \sigma} + D_w + K_H \nabla^4 w$$

$$\frac{\partial \pi'}{\partial t} + \frac{\overline{c}^2}{C_p \overline{\rho} \overline{\theta}_v^2} (D_3) = -u \frac{\partial \pi'}{\partial x} - v \frac{\partial \pi'}{\partial y} - \dot{\sigma} \frac{\partial \pi'}{\partial \sigma}$$
$$- \frac{R_d \overline{\pi}}{c_v} \nabla_3 \bullet \mathbf{V} + \frac{c^2}{C_p \theta_v^2} \frac{d\theta_v}{dt} \quad (0.46)$$

$$\frac{\partial \theta}{\partial t} = -u \frac{\partial \theta}{\partial x} - v \frac{\partial \theta}{\partial y} - \dot{\sigma} \frac{\partial \theta}{\partial \sigma} + \frac{Q_\theta}{\rho} + D_\theta$$
$$+ K_H \nabla^4 (\theta - \theta_{std}) \quad (0.47)$$

$$\frac{\partial e}{\partial t} = -u \frac{\partial e}{\partial x} - v \frac{\partial e}{\partial y} - \dot{\sigma} \frac{\partial e}{\partial \sigma} + BP + SP$$
$$+ D_e + K_B \nabla^4 e - \varepsilon \quad (0.48)$$

$$\frac{\partial q_v}{\partial t} = -u \frac{\partial q_v}{\partial x} - v \frac{\partial q_v}{\partial y} - \dot{\sigma} \frac{\partial q_v}{\partial \sigma} + D_{q_v}$$
$$+ K_H \nabla^4 (q_v - q_v^*) + \frac{S_v}{\rho} \quad (0.49)$$

$$\frac{\partial q_c}{\partial t} = -u \frac{\partial q_c}{\partial x} - v \frac{\partial q_c}{\partial y} - \dot{\sigma} \frac{\partial q_c}{\partial \sigma} + D_{q_c}$$
$$+ K_H \nabla^4 q_c + \frac{S_c}{\rho} \quad (0.50)$$

$$\frac{\partial q_r}{\partial t} = -u \frac{\partial q_r}{\partial x} - v \frac{\partial q_r}{\partial y} - \dot{\sigma} \frac{\partial q_r}{\partial \sigma} + \frac{G_z}{\overline{\rho}} \frac{\partial}{\partial \sigma} (\overline{\rho} V_r q_r)$$
$$+ D_{q_r} + K_H \nabla^4 q_r + \frac{S_r}{\rho} \quad (0.51)$$

$$\frac{\partial q_i}{\partial t} = -u \frac{\partial q_i}{\partial x} - v \frac{\partial q_i}{\partial y} - \dot{\sigma} \frac{\partial q_i}{\partial \sigma} + D_{q_i}$$
$$+ K_H \nabla^4 q_i + \frac{S_i}{\rho} \quad (0.52)$$

$$\frac{\partial q_s}{\partial t} = -u \frac{\partial q_s}{\partial x} - v \frac{\partial q_s}{\partial y} - \dot{\sigma} \frac{\partial q_s}{\partial \sigma} + \frac{G_z}{\overline{\rho}} \frac{\partial}{\partial \sigma} (\overline{\rho} V_s q_s)$$
$$+ D_{q_s} + K_H \nabla^4 q_s + \frac{S_s}{\rho} \quad (0.53)$$

The above equations were determined from the equation of state

$$p = \rho R_d T_v \qquad (0.54)$$

the definition of the virtual temperature

$$T_v = T(1.0 + 0.608 q_v) \qquad (0.55)$$

and the Exner function

$$\pi = \left(\frac{p}{p_{00}} \right)^{R_d / C_p} \qquad (0.56)$$

where

$$\dot{\sigma} = G_x u + G_y v + G_z w \qquad (0.57)$$

$$G_x = \frac{\partial \sigma}{\partial x} = \left(\frac{\sigma - z_{\text{top}}}{z_{\text{top}} - z_{\text{sfc}}} \right) \frac{\partial z_{\text{sfc}}}{\partial x} \qquad (0.58)$$

$$G_y = \frac{\partial \sigma}{\partial y} = \left(\frac{\sigma - z_{\text{top}}}{z_{\text{top}} - z_{\text{sfc}}} \right) \frac{\partial z_{\text{sfc}}}{\partial y} \qquad (0.59)$$

$$G_z = \frac{\partial \sigma}{\partial z} = \frac{z_{\text{top}}}{z_{\text{top}} - z_{\text{sfc}}} \qquad (0.60)$$

For the above equations, p is the pressure; ρ the density; R_d the gas constant for dry air; T the temperature; q_v, q_c, q_r, q_i, and q_s the mixing ratios of water vapor, cloud droplets, raindrops, ice crystals, and snowflakes, respectively; p_{00} a constant reference pressure; C_p the specific heat at constant pressure for the atmosphere; $u, v,$ and w the wind components in the $x, y,$ and z directions, respectively; f the Coriolis force; g the acceleration due to gravity; $S_v, S_c, S_r, S_i,$ and S_s sources and sinks of q_v, q_c, q_r, q_i, and q_s, respectively; Q_θ sources and sinks of heat; V_r and V_s the terminal

69

velocities of raindrops and snowflakes, respectively; θ_{std} the standard atmospheric temperature; q_v^* the standard mixing ratio corresponding to the standard atmospheric temperature; and D_3 the density and potential temperature-weighted three-dimensional divergence,

$$
D_3 = \left(\frac{\partial}{\partial x} + G_x \frac{\partial}{\partial \sigma} \right) \left(\overline{\rho}\overline{\theta}_v u \right) + \left(\frac{\partial}{\partial y} + G_y \frac{\partial}{\partial \sigma} \right) \left(\overline{\rho}\overline{\theta}_v v \right)
$$
$$
+ G_z \frac{\partial \left(\overline{\rho}\overline{\theta}_v w \right)}{\partial \sigma}.
$$
(0.61)

The speed of sound for the mean state, $\overline{c}$, is defined as

$$
\overline{c} = \left(\frac{C_p R_d \overline{\pi}\overline{\theta}_v}{C_v} \right)^{1/2}
$$
(0.62)

where C_v is the specific heat at constant volume for the atmosphere. In equations (0.43)-(0.53) and (0.62), the prognostic variables π and θ have been decomposed as

$$
\pi = \overline{\pi} + \pi'
$$
$$
\theta = \overline{\theta} + \theta'
$$
(0.63)

where the overbar denotes the initial mean state, which is a function of z only, and the prime denotes deviations from the mean. The mean state follows the hydrostatic relationship

$$
G_z \frac{\partial \overline{\pi}}{\partial \sigma} = -\frac{g}{C_p \overline{\theta}_v}.
$$
(0.64)

For a complete description of equations used in the COAMPS model, see Hodur, 1997.

70

APPENDIX D

HPC DISTRIBUTED CENTER WORK-PLAN

PROJECT: COAMPS OPERATIONAL CONFIGURATION TESTING

I.   OBJECTIVE

A limited area model (LAM) is formulated so as to obtain temporal changing synoptic information via lateral boundary conditions from a global forecast model. The temporal frequency and LAM grids over which the energy exchange occurs between the two models has to be fine-tuned so that large- and short-wave synoptic features from the global model propagate appropriately to the LAM. Currently, FNMOC runs COAMPS operationally as a nested LAM. The lateral boundary conditions to the COAMPS outer (coarse) grid are provided at every coarse grid time-step by linearly interpolating global NOGAPS forecast information, which are input for every three hour COAMPS forecast interval. Although this formulation has been giving satisfactory COAMPS forecasts, it is of interest to determine if such forecasts can be improved by: (i) increasing the sampling frequency of the NOGAPS fields to one hour; (ii) changing the relative distance between COAMPS inner nest and its coarse grid boundary where the lateral boundary conditions are introduced; or (iii) running the COAMPS forecasts in a warm start mode to reduce phase errors for synoptic events.

These model runs will be conducted to determine if synoptic meteorological conditions (and therefore mesoscale conditions) are better posed with any of the test scenarios outlined above over what is obtained with the operational setup. NOGAPS fields run specifically to generate lateral boundaries for these COAMPS tests will be used as "truth" for these simulations as it is assumed that one-way COAMPS forecasts of synoptic conditions can be no more accurate than those obtained from NOGAPS. At the same time, a fourth (iv) experiment will be conducted whereby the outer large scale COAMPS nest is dropped and thus, the lateral boundary conditions from NOGAPS are input directly to the current inner nest. This has a potential cost saving and will be tested to determine what, if any, deterioration in the forecast is observed from this setup. A fifth COAMPS configuration will test the impact of extending the current operational L30 configuration to L40.

It is proposed that six parallel numerical simulations be completed to evaluate each of the scenarios mentioned previously. Verification of the results will be conducted to determine the accuracy of both synoptic and mesoscale weather patterns. This will then provide a first step towards optimizing both the NOGAPS sampling frequency and COAMPS operational configuration with the goal of producing the most accurate forecasts possible within given operational constraints.

II.   BACKGROUND

From long experience running NOGAPS operationally at FNMOC, features of traveling waves of periods as small as an hour have been observed. Such short wave features are capable

of impacting weather in local areas. If configured properly, COAMPS would be expected to resolve such weather patterns. However, it has been observed that COAMPS forecasts occasionally miss entirely, or do not resolve well such fast moving synoptic short wave features. This problem is common to all LAM forecasts and is a result of the imperfect treatment of boundary conditions in the models.

One of the largest sources of errors in using boundary information for the LAM is the relatively coarse temporal frequency for which synoptic information is transferred to the LAM. Typically at FNMOC, NOGAPS forecast boundary information is transferred to COAMPS at a three hour forecast interval. However, in the past, NOGAPS boundary conditions have been provided to the COAMPS model at 12 hour intervals. Through a set of sensitivity experiments conducted by the Naval Research Laboratory (NRL), significant COAMPS forecast improvements were observed when the temporal frequency of the NOGAPS boundary conditions were increased to three hours. However, the impact of increasing these boundary conditions to one hour has never been explored.

In addition to the temporal frequency issue, there has been interest in determining if the size and location of the coarsest grid could impact the accuracy of the forecasts produced by a LAM. It is a common practice for LAM models to employ grid structures extending as far upstream from the inner grids as possible. This is done to lessen the impact of the imperfect boundary condition treatment on the finer scale grids interior to this coarsest grid. However, Cliff Mass (University of Washington) in a recent discussion with FNMOC/NRL suggested that the real-time MM5 forecasts conducted at the University of Washington show marked improvement in the synoptic patterns reproduced by MM5 when its coarsest meteorological MM5 grid is located as close to the interior grids as possible.

A third issue to be explored centers around the use of warm starting COAMPS forecasts every watch as is done for the MM5 forecasts at AFWA. The potential advantage to this is a reduction in synoptic scale phase errors due to the initialization of the large scale from NOGAPS every watch. This might lead to better forecasts of synoptic scale meteorological conditions but has the potential disadvantage of a loss of mesoscale forecast information.

The fourth issue to be examined is one posed by NRL. This issue is a cost cutting measure only as it involves the elimination of the coarsest resolution COAMPS nest. The elimination of the coarsest nest would lead to applying the NOGAPS three hour boundary conditions directly to a finer scale nest.   The downside of this recommendation would be the potential degradation in the forecast due to the mismatch in scale between the NOGAPS boundary conditions being input and the scale represented by an interior COAMPS grid. This becomes more pronounced as the interior COAMPS grid uses higher resolution grids as it will resolve more mesoscale features not represented by the large scale global model.

The fifth issue to be explored is an examination of the impact of increasing the vertical resolution within the COAMPS forecasts run at FNMOC. This is a continuation of previous work in which the number of vertical grids employed by the model was extended from 30 to 40 levels. This has been shown by NRL to more realistically transport wave energy aloft in the model. However, testing by FNMOC for cases involving summertime conditions over CONUS indicated that there was little impact by increasing the vertical resolution of the model. However, the lack of significant synoptic forcing in summertime conditions over CONUS might have

skewed the results for these cases. Therefore, these sets of forecasts will be used to examine the impact of the increased resolution for wintertime conditions.

III.   PROJECT PLAN:

This project is projected to take approximately 6-9 months to complete and involve a number of FNMOC personnel. Europe has been chosen as the COAMPS area to be studied due to its importance to Navy Fleet activities, the diversity and frequency of mesoscale weather events observed, and the large number of observations (which can be used in the validation of the results). The project will involve two phases outlined below. The area coverage by the grid used in this project will closely match the existing operational European coverage. However, the test areas will employ a higher resolution 54/18km grid structure and will therefore, not match exactly the geometries used currently in operations. The choice was made to use this higher resolution domain due to FNMOC plans to switch all COAMPS area meteorological grids to this structure in the near future.

Phase I. Daily Model Runs

A set of six separate meteorological forecasts will be run to evaluate each of the scenarios discussed previously. COAMPS meteorological forecasts for each of the five cases will be run beginning 15 December 2003 and continuing through 15 March 2004. NOGAPS boundary conditions will be provided by the beta NOGAPS forecasts running on the operational AMS1/2 machines. Included below is a description of each of the daily forecasts to be run. Each of the forecasts will involve four forecasts per day. Two of the runs will be 48 hours long (real time runs) with the other two being only 6 hours (off time runs). All COAMPS runs will be initialized from the NOGAPS fields and will be run in an unclassified mode. All cases will also involve running the Multivariate Optimal Interpolation (MVOI) model to combine a first guess with available observations from the operational data directories to provide the for COAMPS forecast model with its initial fields.

Base Case

The base case will be set up to mimic the operational run currently conducted at FNMOC. However, as mentioned above, the horizontal resolution of the model will be increased from 81/27/6km to 54/18km. Boundary conditions to be used by the run will be obtained from the three hour real time beta NOGAPS forecast. Operational OCARDS will be used to generate all fields normally produced by the operational run with these fields being stored to a private database. This base case will be run in a "hot start" mode after the initial start up of the model. (The term "hot start" refers to the creation of a first

guess field used by the forecast coming from a previous six hour COAMPS forecast as opposed to obtaining the first guess from NOGAPS forecast fields.)

Experiment 2: Increased temporal boundary conditions

The set up of this run will follow the base case run with the exception of use of additional boundary condition data from the NOGAPS model. For this case, hourly boundary conditions from NOGAPS will be used. As before, the meteorological fields from this forecast will be stored to a separate private database for retention and comparison at a later date

Experiment 3: Coarse Nest Influence

Four experimental runs will be conducted to determine how the lateral separation between the inner nest and its coarse grid affect the COAMPS forecast. The inner nest for all runs will remain unchanged and cover a constant geographical location. The coarse grid will be increased in size in each of the experiments, allowing for a doubling of the lateral separation on the upwind side. The downwind side of the coarse grid (eastern and southern boundaries) will remain the same in each experiment.

Experiment 4: Cold Start

This case will involve obtaining a first guess field for every 12 hour off-time forecast from the NOGAPS forecast fields. Therefore, each real time 48 hour forecast will obtain its first guess fields from a six hour forecast which has been "cold started" from NOGAPS initial conditions. All other elements of this simulation will follow the base case scenario.

Experiment 5: Coarse Grid Elimination

This case will involve the use of an 18 grid only. Boundary conditions for this case will again be developed from the AMS1/2 beta NOGAPS runs. However, the boundary conditions will be applied directly to the 18km grid. The application of these boundary conditions to this grid will be identical to their application to the coarsest grid in the base case (e.g. 3 hour updates linearly interpolated to the 18km grid spacing). All other elements of this simulation will follow the base case scenario.

Experiment 6: Increased vertical resolution

The daily forecasts for this case will involve higher resolution in the vertical than the base case. Most of the new levels will be included in the middle troposphere with only a single level added to the atmosphere below 1500m. All other elements of this simulation will follow the base case scenario.

Roger S will take the lead for this aspect of the project will take an estimated 3 months to complete.

Phase II. Case Study Selection

This phase will take two months to complete and will involve the selection and running of case study days to be modeled; four or five cases will be analyzed. The choice of case study periods will be based on two criteria:

> 1. Subjective analysis of the operational COAMPS Europe gmeta files to identify important synoptic and mesoscale weather events of the region (e.g. Mistral, intense precipitation, etc.);
>
> 2. Identification of significant differences between runs in the validation results from phase I.

These two lists of dates will be developed independently and compared to find common dates on both lists. These results of this comparison will then be used to determine the particular case study days to examine in more detail.

Following the selection of the case study days to be examined, the COAMPS model and fields from each of the Phase I experiments will be used to generate a new 24 hour forecast for the case study days using a high resolution 6km inner nest not run for the daily cases. This inner nest will be tailored to the specific area of interest to determine if higher resolution fields over the area lead to a better forecast of the event. (Validation will again utilize standard observations and therefore, grid placement will also be dependent on the availability of observations in an area.)

Jeff L. will take the lead in determining case study days to be used and Roger S. will be responsible for the associated model runs.

.

Phase III. Model Validation and Verification

There are two levels at which we need to test our hypotheses: Effect of increasing NOGAPS sampling frequency and the effect of emplacing the inner nest closer to the coarse-grid boundary where lateral boundary conditions are introduced, on the (1) propagation of the short- and long-wave phenomenon into the COAMPS forecasts; and (2) improvement in the COAMPS forecasts.

Measuring the improvement in a mesoscale model forecast involves both the subjective and objective verification of sensible weather elements that are routinely measured or estimated (e.g., pressure, temperature, and winds). By increasing the sampling of the lateral boundary conditions, we would expect to see an overall reduction in the phase error of

synoptic and mesoscale disturbances entering the domain. A documented subjective analysis ("man-in-the-loop") of the selected case studies will be carried out to answer questions about phase errors. Of equal importance and to complement the subjective component, an objective verification of the COAMPS forecasts against station observations (or satellite surface winds over the Mediterranean Sea) will demonstrate quantitatively what, if any, improvements are observed both in time and space. Specifically, objective verification will involve:

a) Standard verification statistics of radiosonde observations for Phase I results: both height and time series errors. Past experience running "beta" COAMPS indicates little departure in these type of grid-averaged statistics, however, this information will be supplemented with other parameters and methods of objective verification which may lead to more conclusive results.

b) Surface observation verification will be applied to both Phase I and II results and will be subsampled to zoom in on the area of interest (Phase II results). Parameters to be verified include winds, temperature, and mslp.

c) Remotely sensed surface wind verification: Standard verification scores (e.g., bias, rmse) will be calculated against SSM/I and Quikscat scatterometer maritime winds. Domain subsampling may reveal systematic differences for such areas as Bay of Biscayne or the North Sea (increased LBC frequency and removal of nest1 experiments). Event verification software (Nachamkin, NRL) may also reveal systematic model experiment differences. Contingency table statistics will also be computed to determine any improvement in operationally relevant parameters (Phase I and II results).

d) Raingauge verification: simple differences in forecast-gauge averaged quantity. If data available, It is anticipated that significant experiment differences might be realized with COAMPS L40 forecasts and possibly increased LBC frequency in the form of better wave depiction.

Contributing Sub-Project Proposal

Project Title: COAMPS Lateral Boundary Conditions Simulations

Brief Description: Test to see whether incorporating hourly NOGAPS boundary conditions and/or changes to the operational grid structures improve COAMPS forecasts.

Principal Investigator: Roger Stocker

Collaborator(s): Andy Hergert, Torsten Duffy, Jeff Lerner, Ranjit Passi, Brad Harris (NPS)

Expected start and stop dates: 1 Dec 2003 / 30 June 2003

Relate this project to DC scientific goals: Improve mesoscale forecasting.

What operational transitions are anticipated? Should the results be significantly better using any of the test cases, change operational COAMPS to use these changes.

Infrastructure support requirements:

List Unix account names associated with this sub-project: ahergert, stockerr, duffyt, lernerj, passir, harrisb

Typical model run	On-time	Off-time
# of CPUs:	96	96
Wall clock time:	2:00	:30
# of runs per day:	16	16

Access classified data? No

Request high priority queue (relative to other DC sub-projects)? No

Will most of the AMS3 resources be used in scheduled (near real time) model runs?   Yes

If yes,

Recommended Zulu start time: +4, with forecasts staggered throughout the watch

Major job dependencies (describe, ex: need NOGAPS boundary conditions): NOGAPS boundary conditions (hourly) from NOGAPS beta run on AMS1. This will require code changes to NOGAPS (Duffy).

File system volume written per day, indicate MB/GB/TB

/data (indicate 'MODELS' or 'NRL'): 30 GB for local ISIS files (MODELS)

/scr: 120 GB (MODELS)

/tmp (ops only):

/a/ops/etc/dynamic:
ISIS (indicate alpha/beta/ops):
File system volume 'running' totals, indicate MB/GB/TB
/data (indicate 'MODELS' or 'NRL'): 65 GB (MODELS)
/scr: 250 GB (MODELS)
/tmp (ops only):
/a/ops/etc/dynamic:
ISIS (indicate alpha/beta/ops):

Total Project Long Term Retention (Silo)
/data (indicate 'MODELS' or 'NRL', MB/GB/TB): 5 TB (MODELS)
Retention Period (mos / yrs / indef): 6 mos
(Note: If indefinite, volume should be per year)

Daily transfers OUT of AMS3 (internal or external):
Volume (MB/GB/TB):
Number of files:
Final system destination:

Daily transfers IN to AMS3 (internal or external):
Volume (MB/GB/TB):
Number of files:
Originating system:

Additional comments, if any:

APPENDIX E

A. DATAHD FILES

Run1	Run3a	Run3b	Run3c	
16	16	16	16	total number of pressure levels
30	30	30	30	total number of full sigma levels
2	2	2	2	map proj.1: mercator,2: lambert, 3: polar, 4:cartesian, 5: spherical
70	70	70	70	1st latitue where map projection intersects the earth
18	18	18	18	2nd latitue where map projection intersects the earth
12	12	12	12	long aligned north-south; used for rotaing lambert or polar projec
45	48	50	51	standard latitude used to set up coarse domain
12	8	4	-2	standard longitude used to set up coarse domain
54000	54000	54000	54000	coarse domain grid spacing (meter) in x direction
54000	54000	54000	54000	coarse domain grid spacing (meter) in y direction
2	2	2	2	maximum number of domains in the forecast
7	7	7	7	real data LBC identifier for nests. 6-PK, 7-Davis
7	7	7	7	lateral boundary conditions for x direction
7	7	7	7	lateral boundary conditions for y direction
1	1	1	1	starting i-coordinate for grid stretching
1	1	1	1	ending i-coordinate for grid stretching
1	1	1	1	fractional amount of stretching
7	7	7	7	---------UNKNOWN---------------
121	131	141	151	number of grid points in the x direction for coarse domain
88	98	108	108	number of grid points in the y direction for coarse domain
1	1	1	1	mother domain i points that defines domain 1 staring (1,1) location
1	1	1	1	mother domain j points that defines domain 1 staring (1,1) location
61	66	71	76	coarse domain i points that defines coarse domain standard lat
44	49	54	54	coarse domain j points that defines coarse domain longitude
1	1	1	1	---------UNKNOWN---------------
54000	54000	54000	54000	domain 1 i-grid horizontal resolution
54000	54000	54000	54000	domain 1 j-grid horizontal resolution
16	15	12	10	latitude of domain 1 staring (1,1) location
0	0	0	0	longitude of domain 1 staring (1,1) location
16	16	16	18	latitude of domain 1 lower right corner
43	43	43	43	longitude of domain 1 lower right corner
68	73	77	78	latitude of domain 1 ending (m,n) location
360	360	360	360	longitude of domain 1 ending (m,n) location
55	55	53	47	latitude of domain 1 upper left corner
310	297	284	279	longitude of domain 1 upper left corner
1	1	1	1	---------UNKNOWN---------------
1	1	1	1	---------UNKNOWN---------------
2	2	2	2	---------UNKNOWN---------------

Run1	Run3a	Run3b	Run3c	
295	295	295	295	number of grid points in the x direction for domain 2
196	196	196	196	number of grid points in the y direction for domain 2
12	22	32	44	mother domain i points that defines domain 2 staring (1,1) location
12	12	12	12	mother domain j points that defines domain 2 staring (1,1) location
148	133	118	97	domain 2 i points that defines centerdomain latitude
97	112	127	127	domain 2 j points that defines centerdomain longitude
1	1	1	1	--------UNKNOWN---------------
18000	18000	18000	18000	domain 2 i-grid horizontal resolution
18000	18000	18000	18000	domain 2 j-grid horizontal resolution
23	23	23	24	latitude of domain 2 staring (1,1) location
0	0	0	0	longitude of domain 2 staring (1,1) location
23	23	23	24	latitude of domain 2 lower right corner
40	40	40	40	longitude of domain 2 lower right corner
63	63	63	64	latitude of domain 2 ending (m,n) location
360	360	360	360	longitude of domain 2 ending (m,n) location
54	54	54	55	latitude of domain 2 upper left corner
324	324	324	323	longitude of domain 2 upper left corner
2	2	2	2	--------UNKNOWN---------------
7500	7500	7500	7500	vertical grid spacing level 01
5800	5800	5800	5800	vertical grid spacing level 02
4200	4200	4200	4200	vertical grid spacing level 03
2500	2500	2500	2500	vertical grid spacing level 04
1000	1000	1000	1000	vertical grid spacing level 05
1000	1000	1000	1000	vertical grid spacing level 06
750	750	750	750	vertical grid spacing level 07
750	750	750	750	vertical grid spacing level 08
750	750	750	750	vertical grid spacing level 09
750	750	750	750	vertical grid spacing level 10
750	750	750	750	vertical grid spacing level 11
750	750	750	750	vertical grid spacing level 12
1000	1000	1000	1000	vertical grid spacing level 13
1000	1000	1000	1000	vertical grid spacing level 14
1000	1000	1000	1000	vertical grid spacing level 15
1000	1000	1000	1000	vertical grid spacing level 16
800	800	800	800	vertical grid spacing level 17
800	800	800	800	vertical grid spacing level 18
800	800	800	800	vertical grid spacing level 19
600	600	600	600	vertical grid spacing level 20
400	400	400	400	vertical grid spacing level 21
300	300	300	300	vertical grid spacing level 22
200	200	200	200	vertical grid spacing level 23
140	140	140	140	vertical grid spacing level 24
90	90	90	90	vertical grid spacing level 25
60	60	60	60	vertical grid spacing level 26

Run1	Run3a	Run3b	Run3c	
40	40	40	40	vertical grid spacing level 27
30	30	30	30	vertical grid spacing level 28
20	20	20	20	vertical grid spacing level 29
20	20	20	20	vertical grid spacing level 30
31050	31050	31050	31050	sigmma level (meter) 01
24400	24400	24400	24400	sigmma level (meter) 02
19400	19400	19400	19400	sigmma level (meter) 03
16050	16050	16050	16050	sigmma level (meter) 04
14300	14300	14300	14300	sigmma level (meter) 05
13300	13300	13300	13300	sigmma level (meter) 06
12425	12425	12425	12425	sigmma level (meter) 07
11675	11675	11675	11675	sigmma level (meter) 08
10925	10925	10925	10925	sigmma level (meter) 09
10175	10175	10175	10175	sigmma level (meter) 10
9425	9425	9425	9425	sigmma level (meter) 11
8675	8675	8675	8675	sigmma level (meter) 12
7800	7800	7800	7800	sigmma level (meter) 13
6800	6800	6800	6800	sigmma level (meter) 14
5800	5800	5800	5800	sigmma level (meter) 15
4800	4800	4800	4800	sigmma level (meter) 16
3900	3900	3900	3900	sigmma level (meter) 17
3100	3100	3100	3100	sigmma level (meter) 18
2300	2300	2300	2300	sigmma level (meter) 19
1600	1600	1600	1600	sigmma level (meter) 20
1100	1100	1100	1100	sigmma level (meter) 21
750	750	750	750	sigmma level (meter) 22
500	500	500	500	sigmma level (meter) 23
330	330	330	330	sigmma level (meter) 24
215	215	215	215	sigmma level (meter) 25
140	140	140	140	sigmma level (meter) 26
90	90	90	90	sigmma level (meter) 27
55	55	55	55	sigmma level (meter) 28
30	30	30	30	sigmma level (meter) 29
10	10	10	10	sigmma level (meter) 30
10	10	10	10	pressure level (mb) 01
20	20	20	20	pressure level (mb) 02
30	30	30	30	pressure level (mb) 03
50	50	50	50	pressure level (mb) 04
70	70	70	70	pressure level (mb) 05
100	100	100	100	pressure level (mb) 06
150	150	150	150	pressure level (mb) 07
200	200	200	200	pressure level (mb) 08
250	250	250	250	pressure level (mb) 09
300	300	300	300	pressure level (mb) 10

Run1	Run3a	Run3b	Run3c	
400	400	400	400	pressure level (mb) 11
500	500	500	500	pressure level (mb) 12
700	700	700	700	pressure level (mb) 13
850	850	850	850	pressure level (mb) 14
925	925	925	925	pressure level (mb) 15
1000	1000	1000	1000	pressure level (mb) 16
31055	31055	31055	31055	standard atmospheric height, level 01
26482	26482	26482	26482	standard atmospheric height, level 02
23849	23849	23849	23849	standard atmospheric height, level 03
20576	20576	20576	20576	standard atmospheric height, level 04
18442	18442	18442	18442	standard atmospheric height, level 05
16180	16180	16180	16180	standard atmospheric height, level 06
13609	13609	13609	13609	standard atmospheric height, level 07
11784	11784	11784	11784	standard atmospheric height, level 08
10363	10363	10363	10363	standard atmospheric height, level 09
9164	9164	9164	9164	standard atmospheric height, level 10
7186	7186	7186	7186	standard atmospheric height, level 11
5575	5575	5575	5575	standard atmospheric height, level 12
3012	3012	3012	3012	standard atmospheric height, level 13
1457	1457	1457	1457	standard atmospheric height, level 14
762	762	762	762	standard atmospheric height, level 15
111	111	111	111	standard atmospheric height, level 16

LIST OF REFERENCES

Davies, H.C., 1976: A lateral boundary formulation for multi-level prediction models. *Quart. J. R. Met. Soc.,***102**, 405-418.

Doyle, J., Aug 2004: "Davies vs Perkey-Kreitzberg". Email between LT Brad G Harris and Dr James Doyle discussing why the Davies method is the preferred LBC technique for the COAMPS model.

FNMOC, cited 2004: COAMPS Performance, Tendencies and Feedback. [Available online at https://www.fnmoc.navy.mil/DOD/COAMPS/PERFORMANCE/EUROPE/euroe_p2perform.html] *Last Modified:2211Z 21-Jan-2000*

Hodur, R.M., 1997: The Naval Research Laboratory's Coupled Ocean/Atmospheric Mesoscale Prediction System (COAMPS). *Mon. Wea. Rev.,* **125**, 1414-1430.

Hogan, T.F., and T.E. Rosmond, 1991: The Description of the U.S. Navy Operational Global Atmospheric Prediction System's spectral forecast model. *Mon. Wea. Rev.,* **119,** 1786-1815.

Holton, James R, 1972: *An Introduction to Dynamic Meteorology,* 3d ed. Academic Press, 5-56 pp.

Perkey, D.J., and C.W. Kreitzberg, 1976: A time-dependent lateral boundary scheme for limited-area primitive equation models. *Mon. Wea. Rev.,* **104,** 744-755.

Warner, T.T., R.A. Peterson, and R.E. Treadon, 1997: A Tutorial on Lateral Boundary Conditions as a Basic and Potentially Serious Limitation to Regional Numerical Weather Prediction. *Bull. Amer. Meteor. Soc.,* **78,** 2599-2617.

THIS PAGE INTENTIONALLY LEFT BLAN

INITIAL DISTRIBUTION LIST

1.   Defense Technical Information Center
     Ft. Belvoir, Virginia

2.   Dudley Knox Library
     Naval Postgraduate School
     Monterey, California

3.   Douglas K. Miller
     University North Carolina, Ashville
     Ashville, North Carolina

4.   Beny Neta
     Naval Postgraduate School
     Monterey, California

5.   Clyde Scandrett
     Naval Postgraduate School
     Monterey, California

6.   Philip A. Durkee
     Naval Postgraduate School
     Monterey, California

7.   Roger Stoker
     Fleet Numerical Meteorology and Oceanography Center
     Monterey, California

8.   Brad G. Harris
     Naval Postgraduate School
     Monterey, California

9.   Wendell Nuss
     Naval Postgraduate School
     Monterey, California

10. Bob Creasey
     Naval Postgraduate School
     Monterey, California

11.	Don Walters
	Naval Postgraduate School
	Monterey, California

12.	Jim Doyle
	Naval Research Laboratories - Monterey Regional
	Monterey, California